10

Calcium imaging

FRITJOF HELMCHEN

Over the past 30 years calcium-sensitive fluorescent dyes have emerged as powerful tools for optical imaging of cell function. Calcium ions subserve a variety of essential functions in all cell types. For example, changes in intracellular free calcium concentration ($[Ca^{2+}]_i$) underlie fundamental cellular processes such as muscle contraction, cell division, exocytosis, and synaptic plasticity. Most of these processes rely on the steep gradient of calcium ion concentration that is actively maintained across the plasma membrane. Moreover, cells store calcium ions in intracellular organelles, enabling them to release a surge of Ca^{2+} into the cytosol where and when needed. Calcium ions act through molecular binding to various Ca^{2+}-binding proteins, inducing conformational changes and thereby activating or modulating protein function. The development of optical reporters of calcium concentration has opened great opportunities to read out $[Ca^{2+}]_i$ directly as a crucial intracellular messenger signal. A major application of calcium indicators is the quantitative study of a specific calcium-dependent process X, for example, neurotransmitter release, with the goal to reveal the function $X = X([Ca^{2+}]_i)$. However, this is not the only type of application. Because neuronal excitation in the form of receptor activation or generation of action potentials typically is linked to calcium influx, calcium indicators are also used to reveal neural activation patterns, either within the dendritic tree of individual cells or within cell populations.

Today, a large palette of fluorescent calcium indicators is available. All of them act through binding of Ca^{2+}. In the simplest case the fluorescence intensity depends on $[Ca^{2+}]_i$ but there are several other fluorescence parameters that may change and that can be read out. In order to understand fully the action of calcium ions within cells we need to understand the spatiotemporal dynamics of the variable $[Ca^{2+}]_i(\boldsymbol{x}, t)$ and the complex interactions of Ca^{2+} with Ca^{2+}-binding partners. In particular, we need to consider the calcium indicator itself as one of the interacting reaction partners. For simplicity we will use the notation $[Ca](\boldsymbol{x}, t)$ for the

Handbook of Neural Activity Measurement, ed. Romain Brette and Alain Destexhe. Published by Cambridge University Press.

intracellular free calcium concentration, where the vector $\boldsymbol{x} = (x, y, z)$ refers to the three-dimensional spatial coordinates and t is the temporal variable. It may seem a daunting task to keep track of calcium dynamics throughout a cell but fortunately such detail often is not necessary and various useful mathematical models can be derived based on reasonable simplifications. A fundamental aspect that the experimenter should be aware of is the fact that calcium indicators inevitably perturb intracellular calcium dynamics (to a lesser or greater degree). This notion means that indicators interfere with the variable they are supposed to report, which may limit the information that can be gathered. On the flipside, knowledge about how calcium indicators influence intracellular calcium dynamics can be exploited by the experimenter as we will discuss in this chapter. Being familiar with the principles of how calcium indicators work and with the mathematical description of calcium dynamics thus is essential for the design and interpretation of calcium imaging experiments.

The chapter starts with a brief introduction of the different types of fluorescent calcium indicators. Subsequently, the fundamental processes involved in intracellular calcium dynamics and their mathematical descriptions are introduced. To help the reader a list of key parameters used in the mathematical description is provided in Table 10.1. Following a treatment of the Ca^{2+}-dependence of fluorescence we then discuss simplified models of calcium dynamics and their applications to reveal specific aspects of neural dynamics. The chapter concludes with a brief comparison with other methods and a discussion of future perspectives.

10.1 Fluorescent calcium indicators

The first optical $[Ca^{2+}]_i$ measurements were achieved in the 1960s and 1970s using the bioluminescent protein Aequorin (e.g. Ridgway and Ashley, 1967) or metallochromic arsenazo dyes that change their light absorbance depending on $[Ca^{2+}]_i$ (e.g. Brown et al., 1975). Although these indicators are still sometimes used we focus here entirely on fluorescent calcium indicators, the prevailing indicator form today. Fluorescence readout is beneficial because even at low indicator concentrations it allows for high-contrast labeling against a low background (Tsien, 1989). Two different types of fluorescent calcium indicators exist (Figure 10.1): (1) small-molecule indicators (SMIs), which are synthetic organic dyes that have been developed since the beginning of the 1980s (Tsien, 1980); and (2) calcium-sensitive fluorescent proteins, the first one of which was reported in 1997 (Miyawaki et al., 1997). The latter type often is referred to as the group of genetically-encoded calcium indicators (GECIs). It is beyond the scope of this chapter to provide a complete overview of the various indicator types and the history of their development (for detailed reviews see Tsien, 1989; Miyawaki, 2003; Garaschuk et al., 2007;

Table 10.1 *Key parameters of intracellular calcium dynamics and fluorescent calcium indicators.*

Parameter	Definition	Typical range/unit
$[Ca^{2+}]_i$ or [Ca]	intracellular free Ca^{2+} concentration, in general space and time dependent	50 nM–100 μM
$[Ca^{2+}]_{rest}$	resting intracellular free Ca^{2+} concentration	50–150 nM
k_{on}	association rate constant of Ca^{2+} binding	10^6–10^9 M^{-1} s^{-1}
k_{off}	dissociation rate constant of Ca^{2+} binding	1–10^3 s^{-1}
K_d	dissociation constant of a Ca^{2+} binding molecule	100 nM–0.1 mM
κ_B	Ca^{2+} binding ratio, "strength of buffering"	10–1000 for endogenous buffers
κ_m	Ca^{2+} binding ratio of a mobile buffer	
κ_f	Ca^{2+} binding ratio of an immobile ("fixed") buffer	
j_{in}	concentration change due to Ca^{2+} influx	M s^{-1}
j_{out}	concentration change due to Ca^{2+} extrusion	M s^{-1}
j_{leak}	leakage term to maintain $[Ca^{2+}]_{rest}$	M s^{-1}
F	Faraday's constant	96485 C mol^{-1}
Q_{Ca}	"calcium charge," related to total number of calcium ions entering a cell during influx	C
v_{max}	maximum velocity of a Ca^{2+} extrusion pump	mol m^{-2} s^{-1}
γ	linear extrusion rate of a simplified extrusion mechanism	100–2000 s^{-1}
D_{Ca}	diffusion constant of free calcium ions	220 μm^2 s^{-1}
$D_{B,i}$	diffusion constant of Ca^{2+} binding molecule species i	μm^2 s^{-1}
D_{app}	apparent diffusion constant in the presence of Ca^{2+} binding molecules	μm^2 s^{-1}
ε	molar dye extinction coefficient	20 000–100 000 M^{-1} cm^{-1}
Q_F	quantum yield	between 0 and 1
Q_D	quantum efficiency of a photodetector	0–100%, typically between 10–40%
R_f	dynamic range of an indicator	
τ_F	fluorescence lifetime of an indicator	1–10 ns
Φ_D	collection efficiency of the detector system	0–100%, typically far less than 100%
(K_{eff}, R_{min}, R_{max})	triplet of calibration parameters for ratiometric measurements	
(K_d, $\Delta F/F_{max}$, $[Ca^{2+}]_{rest}$)	triplet of calibration parameters for single-wavelength measurements	
(K_d, R_f, F_{max})	alternative triplet of calibration parameters for single-wavelength measurements	
(K_{app}, τ_{min}, τ_{max})	triplet of calibration parameters for fluorescence lifetime measurements	

Mank and Griesbeck, 2008). Nonetheless, it is useful to illustrate briefly how these indicator molecules work before we start the mathematical treatment.

10.1.1 Small-molecule indicators

The first type of calcium indicators are small organic molecules. A major step in their development was the modification of the well-known Ca^{2+}-chelating molecule EGTA to BAPTA, a Ca^{2+} chelator with fast binding kinetics (Tsien, 1980). Many of the SMIs are designed by covalently attaching a fluorophore to the BAPTA-derived Ca^{2+} chelating part. As an example, Oregon Green BAPTA-1 is shown in Figure 10.1A. Binding of Ca^{2+} to the octacoordinate pocket of the chelator leads to a reconfiguration of the conjugated electron system, which then induces changes in the fluorescence properties. The exact nature as well as the strength of the fluorescence changes can be tuned by the choice of the

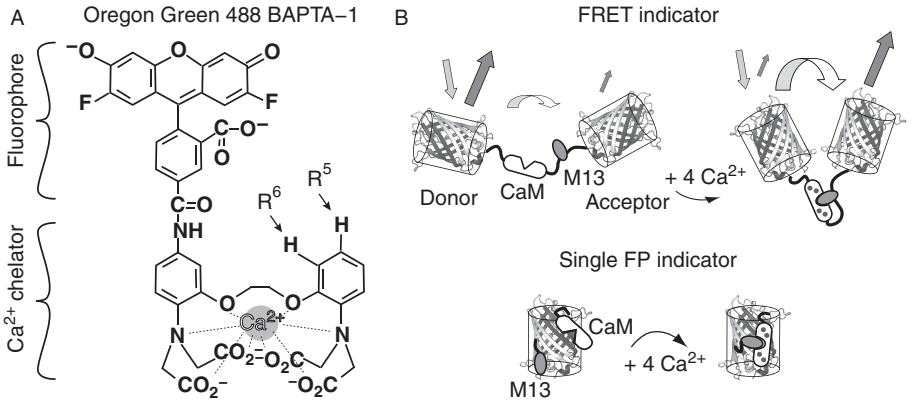

Figure 10.1 Examples of the two major classes of fluorescent calcium indicators. A. Oregon Green BAPTA-1 is a small-molecule indicator consisting of a Ca^{2+}-chelating part and a fluorophore part. Variants of Oregon Green BAPTA indicators differ in their substituents at key positions: Oregon Green BAPTA-5N contains a nitro group at position R^5 and Oregon Green BAPTA-6F a contains fluorine atom at position R^6. B. Genetically encoded calcium indicators are further subdivided into two classes. Top: FRET-based indicators rely on the Ca^{2+}-dependent change in distance between two fluorescent proteins, mediated by a Ca^{2+}-binding linker (here Calmodulin which binds four calcium ions and interacts with the M13 peptide). One fluorescent protein acts as donor, the other as acceptor for FRET. FRET efficiency increases when the two proteins are brought closer together. Bottom: Ca^{2+}-binding domains are incorporated into single circularly permutated fluorescent proteins. In these single-protein indicators Ca^{2+}-binding leads to a conformational change that is sensed by the chromophore inside the fluorescent protein barrel structure, causing a change in fluorescence intensity.

substituents at critical intramolecular positions, so that a multitude of indicator variants can be created. With the exception of some indicators that have been targeted to the membrane by attaching lipophilic side chains, most of the SMIs are water soluble and readily diffuse throughout the cytosol. In their salt form, indicators dissociate in solution. As charged molecules they are not membrane permeable and therefore need to be loaded into cells with special techniques. Direct physical methods include electroporation and filling via intracellular recording pipettes. An elegant alternative method is to load SMIs into cells using their acetomethoxy(AM)-conjugated form (Tsien, 1981). In this chemically modified form the carboxy-groups are esterified and thus turned into uncharged side groups. Consequently, the AM-form of indicators is membrane permeable. Once inside the cytosol, however, the ester-groups are cleaved by endogenous esterases, so that the original indicator molecule is recovered but is now trapped inside the cell. AM-ester loading of calcium has been used for many years to label cells in cell culture and in brain slices. Only recently, bolus injection of AM-indicators directly into neural tissue has enabled labeling of large cell populations in the intact brain (Stosiek et al., 2003). This breakthrough has opened new opportunities for optical recording of neural network activity in vivo (Garaschuk et al., 2006; Göbel and Helmchen, 2007a; Grewe and Helmchen, 2009).

10.1.2 Genetically encoded calcium indicators

The second group of fluorescent calcium indicators is the still rapidly growing group of GECIs. Similar to SMIs, a large variety of GECIs is available. Two major classes can be distinguished (Figure 10.1B). In the first class, GECIs are designed by coupling two fluorescent proteins (e.g. cyan fluorescent protein, CFP, and yellow fluorescent protein, YFP) via a Ca^{2+}-binding linker. Due to their enforced close proximity the two proteins can exchange energy via fluorescence resonance energy transfer (FRET) (Stryer, 1978). One protein acts as acceptor and the other as donor molecule. Ca^{2+}-binding to the linker induces a conformational change that brings the two proteins closer together. Because of the strong distance dependence of FRET, this leads to a change in the fluorescence emissions of the two proteins that can be read out ratiometrically (see below). The first constructs of this kind used the Ca^{2+}-dependent interaction of calmodulin (CaM) with the M13 protein domain to translate $[Ca^{2+}]_i$ changes into FRET changes (Miyawaki et al., 1997). Meanwhile many variants of such "chameleons" have been generated (Nagai et al., 2004; Palmer et al., 2006). In addition, other FRET-based designs have been introduced using the Troponin C protein as Ca^{2+}-dependent linker molecule (Heim and Griesbeck, 2004; Garaschuk et al., 2007).

The second major class of GECIs comprises single-protein indicators rather than tandem pairs of proteins (Figure 10.1B). Example proteins are Inverse Pericam or members of the GCaMP family (Tian et al., 2009). In these indicators, the protein has been modified by insertion of a Ca^{2+}-binding domain such that Ca^{2+}-binding leads to a conformational change that either increases or decreases the fluorescence yield of the chromophore (Baird et al., 1999; Nakai et al., 2001). Compared to SMIs the general advantages of GECIs are the possibilities of long-term expression and of targeting them to specific subtypes of neurons or subcellular locations. Many of the initial problems have now been overcome and one can expect rapid expansion of the application of GECIs for functional measurements in the upcoming years.

10.2 Intracellular calcium dynamics

This section gives a general description of the spatiotemporal dynamics of $[Ca^{2+}]_i$ within a cell before we will treat Ca^{2+}-sensitive fluorescence changes of calcium indicators in the next section. For the main dynamic processes involved in intracellular calcium handling (binding, influx, extrusion, and diffusion) we introduce the key parameters and generic mathematical formulations. First considered individually, we then combine these aspects in a general set of differential equations that describes intracellular calcium dynamics.

10.2.1 Calcium binding

Within the cytosol, calcium ions bind to a multitude of endogenous proteins. In addition, Ca^{2+}-binding is the fundamental process by which calcium indicators work. In the case of Oregon Green BAPTA-1 Ca^{2+}-binding occurs at an octacoordinate binding site of the chelator part (Figure 10.1A). This indicator is an example of one-to-one binding of Ca^{2+} to a molecule. In many proteins, including GECIs, the Ca^{2+}-binding sites are so-called EF-hand domains (Mank and Griesbeck, 2008; Schwaller, 2009), of which several may be present in the protein. For example, calmodulin is made up of four EF-hand domains. These domains are not independent in their structural rearrangements upon Ca^{2+}-binding, resulting in cooperativity of the binding processes. We first consider independent binding before we briefly discuss cooperative binding.

Independent calcium binding In the simplest case calcium ions are bound either individually or, if multiple calcium ions can bind to the molecule, binding events occur independent from each other. In this case we only need to consider the simple binding scheme

$$\mathrm{Ca}^{2+} + \mathrm{B} \underset{k_{off}}{\overset{k_{on}}{\rightleftarrows}} \mathrm{CaB} \tag{10.1}$$

where B denotes the binding site and CaB the calcium-bound complex. B thus stands for an intracellular protein or an exogenous Ca^{2+}-binding molecule that has been artificially introduced into the cell, for example, an indicator dye. Binding occurs with an association rate k_{on} (unit $\mathrm{mM^{-1}s^{-1}}$) and the complex CaB dissociates with a rate k_{off} (unit $\mathrm{s^{-1}}$). The temporal dynamics of this process is described by the following differential equations:

$$\begin{aligned}
\frac{\partial\,[\mathrm{Ca}]}{\partial t} &= -k_{on}\,[\mathrm{Ca}]\,[\mathrm{B}] + k_{off}\,[\mathrm{CaB}] \\
\frac{\partial\,[\mathrm{B}]}{\partial t} &= -k_{on}\,[\mathrm{Ca}]\,[\mathrm{B}] + k_{off}\,[\mathrm{CaB}] \\
\frac{\partial\,[\mathrm{CaB}]}{\partial\,t} &= -\frac{\partial\,[\mathrm{B}]}{\partial t} = k_{on}\,[\mathrm{Ca}]\,[\mathrm{B}] - k_{off}\,[\mathrm{CaB}] \\
[\mathrm{Ca}]_T &= [\mathrm{Ca}] + [\mathrm{CaB}] \\
[\mathrm{B}]_T &= [\mathrm{B}] + [\mathrm{CaB}]\,.
\end{aligned} \tag{10.2}$$

Here, we have introduced the total concentrations $[\mathrm{Ca}]_T$ and $[\mathrm{B}]_T$ as the sum of the free and bound forms. $[\mathrm{Ca}]_T$ is conserved in the absence of Ca^{2+} influx into or extrusion from the cytosol. $[\mathrm{B}]_T$ is conserved unless changes in expression levels of Ca^{2+}-binding proteins occur or exogenous Ca^{2+} buffers are artificially added.

In many cases one is mainly interested in the steady-state concentrations when equilibrium has been reached. In this case the concentration changes on the left hand side are zero. From Equations (10.2) the law of mass action follows, in which the affinity of B for binding Ca^{2+} is described by the dissociation constant

$$K_d = \frac{k_{off}}{k_{on}} = \frac{[\mathrm{Ca}]\,[\mathrm{B}]}{[\mathrm{CaB}]} = \frac{[\mathrm{Ca}]\,([\mathrm{B}]_T - [\mathrm{CaB}])}{[\mathrm{CaB}]}. \tag{10.3}$$

The dissociation constant K_d has the intuitive meaning that it is equal to the $[Ca^{2+}]_i$ level, at which 50% of the binding sites have bound Ca^{2+}. This is obvious by rearranging Equation (10.3) to yield the so-called saturation curve of the binding species B:

$$S = \frac{[\mathrm{CaB}]}{[\mathrm{B}]_T} = \frac{[\mathrm{Ca}]}{[\mathrm{Ca}] + K_d}. \tag{10.4}$$

This saturation curve is plotted in Figure 10.2A. For limited ranges of $[Ca^{2+}]_i$ this curve can be piecewise approximated by a linear function. Note that there is an inverse relationship between the expressions "affinity" and "dissociation constant" with a low K_d value implying a high affinity and vice versa. This notion is

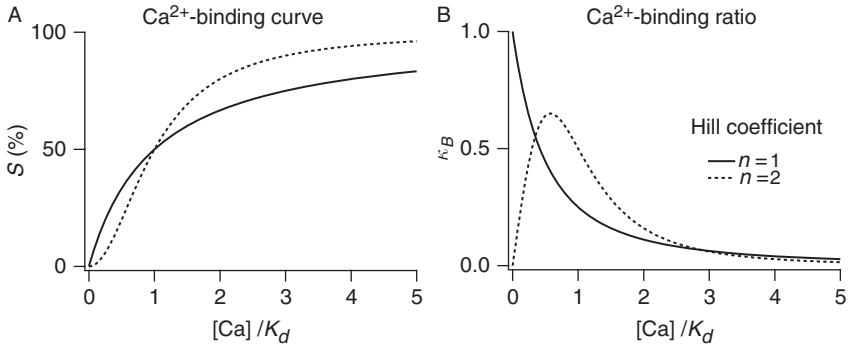

Figure 10.2 Saturation curve and Ca^{2+}-binding ratio for Ca^{2+}-binding molecules showing either independent binding (Hill coefficient $n = 1$) or cooperative binding ($n = 2$). A. Percentage of saturation as a function of calcium concentration level normalized to the dissociation constant. B. Ca^{2+}-binding ratio κ_B as a function of normalized calcium concentration level.

important for working with calcium indicators because the affinity of the indicator should match the expected range of calcium concentrations "seen" by the indicator. Typically, indicators are only sensitive in a narrow window of the entire range of possible intracellular $[Ca^{2+}]_i$ levels that spans from resting concentrations of below 10^{-4} mM to high concentrations around 0.1 mM, which for example can occur locally at sites of calcium influx. If the affinity of the indicator is too low (K_d too high) it will not be sensitive in the low concentration range; if the affinity is too high the indicator will be nearly saturated. Thus, depending on the experimental aims, the most appropriate indicator has to be chosen from the available spectrum of dyes with widely different affinities. High affinity calcium indicators have dissociation constants in the submicromolar range (e.g. K_d of OGB-1 is about 200–300 nM), while K_d values reach around 50 μM for low affinity indicators.

A second important aspect is that the Ca^{2+}-binding efficiency depends on the $[Ca^{2+}]_i$ level. This is intuitively clear as the probability of Ca^{2+}-binding will decrease once a certain number of ions are already bound. In other words, fewer and fewer binding sites will be available until – at relatively high $[Ca^{2+}]_i$ levels – most binding sites are occupied and this particular species of Ca^{2+}-binding molecules becomes saturated. Formally this dependency is expressed by the so-called "Ca^{2+}-binding ratio" κ_B, which is obtained by differentiating Equation (10.4):

$$\kappa_B = \frac{\partial[\mathrm{CaB}]}{\partial[\mathrm{Ca}]} = \frac{[\mathrm{B}]_T K_d}{([\mathrm{Ca}] + K_d)^2}. \tag{10.5}$$

The Ca^{2+}-binding ratio scales with the total concentration of the binding species. For independent calcium binding, κ_B has a maximal value of $[\mathrm{B}]_T / K_d$ at zero

$[Ca^{2+}]_i$ and decreases monotonically for increasing $[Ca^{2+}]_i$ levels (Figure 10.2B). In the literature the Ca^{2+}-binding ratio is also often termed "buffering capacity" or "buffering strength." As we will see further below, the concept of Ca^{2+}-binding ratio is very helpful in describing key aspects of calcium buffers and indicators. In general, it is desirable to know (or at least to have a good estimate of) the Ca^{2+}-binding ratios of both the endogenous calcium buffers and the fluorescent calcium indicator that is used for the measurement.

Cooperative calcium binding While independent Ca^{2+}-binding is a good model for small-molecule calcium indicators, it does not adequately describe the situation for many protein binding reactions. The reason is that Ca^{2+}-binding proteins often contain multiple, structurally connected binding sites that are no longer independent. More generally, we therefore have to consider cooperative binding as it is known from the classic case of O_2-binding to hemoglobin.

A general description of cooperative binding is fairly complex. For our purposes it is sufficient to incorporate cooperativity using the Hill equation, which is an empirical description of the equilibrium case. In this simplified view, binding of multiple calcium ions is described using the Hill coefficient n and an apparent dissociation constant K_A

$$K_A = \frac{[\mathrm{Ca}]^n\,[\mathrm{B}]}{\left[\mathrm{Ca}^n\mathrm{B}\right]} = \frac{[\mathrm{Ca}]^n\,([\mathrm{B}]_T - \left[\mathrm{Ca}^n\mathrm{B}\right])}{\left[\mathrm{Ca}^n\mathrm{B}\right]}. \tag{10.6}$$

Note that the Hill coefficient is not equal to the number of binding sites but rather is an empirical parameter that describes the overall effect of cooperative binding. The saturation curve in this case takes a sigmoidal shape according to the equation

$$S = \frac{\left[\mathrm{Ca}^n\mathrm{B}\right]}{[\mathrm{B}]_T} = \frac{[\mathrm{Ca}]^n}{[\mathrm{Ca}]^n + K_A} = \frac{[\mathrm{Ca}]^n}{[\mathrm{Ca}]^n + K_d^n}, \tag{10.7}$$

where K_d again is the calcium concentration at half-maximal occupancy (Figure 10.2A). Hill coefficients for GECIs are in the range of 0.7–3.8 (Mank and Griesbeck, 2008). From Equation (10.7) we can also derive the Ca^{2+}-binding ratio for the case of cooperative binding:

$$\kappa_B = \frac{\partial\left[\mathrm{Ca}^n\mathrm{B}\right]}{\partial\,[\mathrm{Ca}]} = [\mathrm{B}]_T\,\frac{n\,[\mathrm{Ca}]^{n-1}\,K_d^n}{([\mathrm{Ca}]^n + K_d^n)^2}. \tag{10.8}$$

This relationship is plotted in Figure 10.2B for $n = 2$, showing a non-monotonic $[Ca^{2+}]_i$ dependence of κ_B with a maximum at some intermediate concentration level. This highly non-linear behavior makes the interpretation of calcium measurements with GECIs more difficult so that the binding characteristics of the specific indicator need to be taken into account.

Often Ca^{2+}-binding is referred to as "buffering" and many proteins are classified as "calcium buffers." While "binding" refers to the physical process itself, "buffering" has a functional meaning and refers to the ability of a molecular species to maintain the $[Ca^{2+}]_i$ level within a certain concentration range by dampening changes in free calcium concentration following calcium influx. For a number of proteins, calcium buffering appears to be the main function, although additional Ca^{2+}-sensing functions may be unknown and await to be discovered (Schwaller, 2009).

10.2.2 Calcium influx

The steady-state equilibrium of Ca^{2+} binding and unbinding in the cytosol is continually perturbed by Ca^{2+} influx from various sources (Figure 10.3). For example, neural excitation leads to Ca^{2+} flux across the plasma membrane through either voltage-gated calcium channels or calcium-permeable receptor channels. Moreover, Ca^{2+} may be released from intracellular stores, including the endoplasmic reticulum and mitochondria. In general, we denote the spatially and temporally varying influx as $j_{in}(\mathbf{x}, t)$. In the absence of extrusion mechanisms, the spatiotemporal integral of j_{in} equals the total calcium charge Q_{Ca} that enters the cell during a

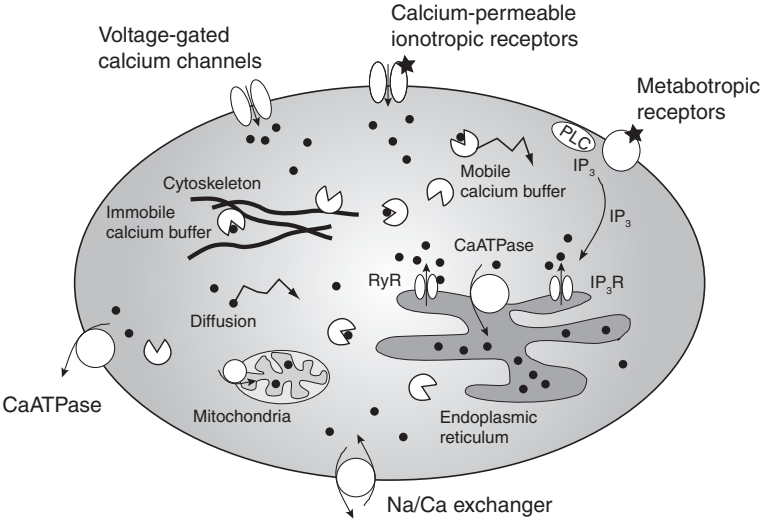

Figure 10.3 Schematic illustration of various processes that contribute to intracellular calcium dynamics. Several pathways exist for entry of calcium ions into the cytosol (black dots), including influx through voltage- or ligand-gated channels and release from intracellular organelles. Intracellularly, calcium ions diffuse and bind to various mobile or immobile Ca^{2+}-binding proteins. Several extrusion mechanisms remove calcium from the cytosol. PLC phospholipase C, RyR ryanodine receptor, IP_3R inositol-tri-phosphate receptor.

given time period. This calcium load will change the total concentration of calcium ions (free or bound), which is given by

$$[\mathrm{Ca}]_T = [\mathrm{Ca}] + \sum_i [\mathrm{CaB}_i]. \tag{10.9}$$

The index i in B_i runs over all Ca^{2+}-binding molecular species that are present. While the spatiotemporal pattern of influx in general is highly complex, approximate expressions can be used for j_{in} in particular situations. For example, if calcium influx is brief compared to extrusion times and if it can be assumed to occur rather homogenously throughout the cell compartment, then j_{in} can be approximated by a pulse-like, instantaneous influx, which can be mathematically expressed by the Kronecker delta function

$$j_{in} = \Delta [\mathrm{Ca}]_T \ \ \delta(t - t_p) = \frac{Q_{Ca}}{2\,F\,V}\ \delta(t - t_p), \tag{10.10}$$

where t_p is the point in time when influx occurs, F is Faraday's constant, and V is the volume of the cell compartment under consideration. This approximation is particularly useful for describing action-potential evoked Ca^{2+} influx, because voltage-gated calcium channels open for less than a millisecond during the repolarizing phase of the action potential (Borst and Helmchen, 1998). Ca^{2+} extrusion in the soma, dendrites or axons is typically at least an order of magnitude slower. For a train of n action potentials, Equation (10.10) can be extended to a sum of delta functions with spike times at time points t_k with $k = 1, \ldots, n$. If Ca^{2+} influx does not occur in a pulse-like way but rather is prolonged, for example, during excitatory postsynaptic currents or during release from intracellular stores, the time course of j_{in} needs to be modeled with other suitable analytical functions.

How is the extra calcium load following Ca^{2+} influx distributed among the Ca^{2+}-binding partners present? After an initial non-equilibrium phase that is governed by binding kinetics and diffusional exchange, a new steady state will be reached. The steady-state concentration *changes* of all partners (expressed with the greek "delta" Δ) depend on each other according to:

$$\Delta [\mathrm{Ca}]_T = \Delta [\mathrm{Ca}] + \sum_i \Delta [\mathrm{CaB}_i] = \Delta [\mathrm{Ca}] + \sum_i \kappa_{B,i} \Delta [\mathrm{Ca}] = \Delta [\mathrm{Ca}] \left(1 + \sum_i \kappa_{B,i}\right). \tag{10.11}$$

Here, we approximated concentration changes of Ca^{2+}-bound molecules with the help of their Ca^{2+}-binding ratios (assuming relatively small changes). We conclude that the change in free calcium concentration is determined by the total change in concentration divided by one plus the sum of all Ca^{2+}-binding ratios:

$$\Delta [\mathrm{Ca}] = \frac{\Delta [\mathrm{Ca}]_T}{(1 + \sum_i \kappa_{B,i})} = \frac{Q_{Ca}}{2\,F\,V} \frac{1}{(1 + \sum_i \kappa_{B,i})}. \tag{10.12}$$

As we will discuss in more detail further below, this equation in particular implies that addition of a calcium indicator to the system may significantly affect changes in free calcium concentration. The magnitude of this effect will, however, also depend critically on the concentrations and properties of all other Ca^{2+}-binding molecules present.

10.2.3 Calcium extrusion

Calcium extrusion is vital for the cell because low $[Ca^{2+}]_i$ levels need to be re-established following surges of Ca^{2+} influx in order to keep the cell alive. Cells maintain a very low resting free calcium concentration through effective calcium pump mechanisms (Figure 10.3). Calcium ions are either sequestered into intracellular organelles or extruded via the plasma membrane until a resting $[Ca^{2+}]_i$ level of about 30–100 nM has been re-established (Helmchen et al., 1996; Maravall et al., 2000). The requirement to keep $[Ca^{2+}]_i$ levels low may have arisen early in evolution because calcium compounds are prone to precipitation. The resulting steep concentration gradient across the membrane then presumably provided opportunities to use Ca^{2+} as a fast and effective signaling ion.

In general terms we denote the spatiotemporal calcium extrusion with $j_{out}(\mathbf{x}, t)$. A common formalization is the description as Ca^{2+}-dependent, saturable mechanism with first-order Michaelis–Menten kinetics:

$$j_{out}([Ca]) = v_{max}\frac{A}{V}\frac{[Ca]}{[Ca] + K_m}, \tag{10.13}$$

where v_{max} is the maximal efflux rate per unit area of cell membrane, A is the compartment surface, and K_m is the concentration at which extrusion is half-maximal. This equation does not account for the fact that $[Ca^{2+}]_i$ is not zero at rest. Under resting conditions a steady state exists between some leakage Ca^{2+} influx and the extrusion of Ca^{2+}, resulting in a zero net flux. Resting conditions are most easily incorporated in the mathematical description of calcium dynamics by including a constant leakage term that just balances the pump mechanisms at rest:

$$j_{leak} = -v_{max}\frac{A}{V}\frac{[Ca]_{rest}}{[Ca]_{rest} + K_m}. \tag{10.14}$$

If the pumps operate well below saturation ($[Ca^{2+}]_i \ll K_m$) the net extrusion can be further simplified by linearization of Equations (10.13) and (10.14) using a single clearance rate γ

$$j_{out}([Ca]) = \gamma\ \Delta[Ca] = \gamma([Ca] - [Ca]_{rest}). \tag{10.15}$$

Because many possible calcium extrusion pathways exist, characterization of calcium dynamics in a particular cell type or cell compartment should first aim to

identify the predominant pathway and then examine whether saturation is reached during the experimental protocol because distinct extrusion mechanisms may dominate at low and high $[Ca^{2+}]_i$ levels. Such investigation, for example using pharmacological tools, can provide a good starting point for adequate modeling of calcium extrusion. As a complicating issue, slow Ca^{2+}-binding mechanisms sometimes operate on a time scale similar to extrusion, which makes it difficult to distinguish between these mechanisms which both represent calcium "sinks" (see below). While extruded Ca^{2+} is lost, slowly bound Ca^{2+} remains in the cytosol and can still shift to other Ca^{2+}-binding partners and exert functional control.

10.2.4 Calcium diffusion

Another important aspect is the spatial distribution and mobility of calcium ions as well as of Ca^{2+}-binding molecules. While some proteins are anchored to the cytoskeleton in strategic places and thus exhibit low mobility, others can diffuse freely throughout the cytosol. As mentioned above, many calcium indicators show a rather high mobility and can fill the entire cell by diffusion. For freely diffusible substances, the concentration is homogenous throughout a given cell compartment at steady state. Localized Ca^{2+} influx and efflux will cause short-lived concentration gradients, which then equilibrate by diffusion. Diffusion is a probabilistic process due to the thermal agitation of molecules. For any diffusible substance S the temporal change of the concentration $[S](\mathbf{x}, t)$ at a position $\boldsymbol{x}$ is given by the difference of influx and efflux in the local volume element, which both depend on the local concentration gradient. For the one-dimensional case the resulting balance equation is the *diffusion equation*

$$\frac{\partial [S](x,t)}{\partial t} = D_S \frac{\partial^2 [S](x,t)}{\partial x^2} \tag{10.16}$$

where D_S is the diffusion coefficient. A characteristic feature of diffusional spread is that the mean displacement $\langle x \rangle$ of the diffusing particles is proportional to the square-root of the time period Δt

$$\langle x \rangle \propto \sqrt{D_S \, \Delta t}. \tag{10.17}$$

For example, a substance with a diffusion coefficient of $100\,\mu m^2\,s^{-1}$ spreads from a point source about 0.3 μm in 1 ms, 1 μm in 10 ms, 3 μm in 100 ms, and 10 μm in 1 s. In cells with elaborate morphologies such as neurons, this square-root-law of diffusion has the important consequence that intracellular chemical signals can be effectively compartmentalized so that their action is restricted to a certain spatial range. For the three-dimensional case we rewrite Equation (10.16) in vector notation. For the diffusion of free calcium ions we write for example

$$\frac{\partial\,[\mathrm{Ca}]\,(\mathbf{x},t)}{\partial t} = D_{Ca}\,\nabla(\nabla\,[\mathrm{Ca}]\,(\mathbf{x},t)), \tag{10.18}$$

where ∇ denotes the gradient operator. We avoid the Laplace operator $\Delta f = \nabla(\nabla f)$ here because of the potential confusion with Δ, the "delta" sign used to express signal changes.

For large molecules (molecular weight $M > 1000$) the diffusion coefficient depends on the molecule radius and hence on the inverse of the cubic root of M. Due to the formation of hydration shells in aqueous solution, ions have relatively small diffusion coefficients. For free calcium ions D_{Ca} is about $600\,\mu\mathrm{m}^2/\mathrm{s}^{-1}$ in water but is reduced to $D_{Ca} \approx 220\,\mu\mathrm{m}^2\,\mathrm{s}^{-1}$ in the cytosol (Allbritton et al., 1992). In general, diffusion coefficients are two to three times lower inside cells compared to in water because of the higher viscosity (Woolf and Greer, 1994). If multiple diffusible molecules are present, each will spread according to its diffusion coefficient. As a consequence the diffusional spread of calcium ions can be either promoted or slowed down in the presence of Ca^{2+}-binding molecules, depending on their mobility (see below). In particular, loading a cell with calcium indicator may affect not only Ca^{2+}-buffering but also the overall diffusional spread of calcium ions.

10.2.5 General formulation of calcium dynamics

We can now give a general description of intracellular calcium dynamics that incorporates all the different aspects of Ca^{2+}-binding, influx, efflux, and diffusion. Assuming the presence of multiple Ca^{2+}-binding molecules B_i we obtain the following set of *reaction-diffusion equations*

$$\begin{aligned}
\frac{\partial\,[\mathrm{Ca}]}{\partial t} &= D_{Ca}\nabla(\nabla\,[\mathrm{Ca}]) - [\mathrm{Ca}]\sum_i k_{on,i}\,[B_i] + \sum_i k_{off,i}\,[\mathrm{CaB}_i] \\
&\quad + j_{in} - j_{out} + j_{leak} \\
\frac{\partial\,[\mathrm{B}_i]}{\partial t} &= D_{B,i}\nabla(\nabla\,[\mathrm{B}_i]) - k_{on,i}\,[\mathrm{Ca}]\cdot[\mathrm{B}_i] + k_{off,i}\,[\mathrm{CaB}_i] \\
\frac{\partial\,[\mathrm{CaB}_i]}{\partial t} &= D_{CaB,i}\nabla(\nabla\,[\mathrm{CaB}_i]) + k_{on,i}\,[\mathrm{Ca}]\cdot[\mathrm{B}_i] - k_{off,i}\,[\mathrm{CaB}_i] \\
[\mathrm{B}_i]_T &= [\mathrm{B}_i] + [\mathrm{CaB}_i] \\
[\mathrm{Ca}]_T &= [\mathrm{Ca}] + \sum_i [\mathrm{CaB}_i].
\end{aligned} \tag{10.19}$$

For each species of Ca^{2+}-binding molecules we have to write three equations analogous to the middle three equations. Note that this formulation can be simplified under the assumptions that (1) the total concentration of mobile binding

partner $[B_i]_T$ is spatially uniform and (2) the diffusion coefficients of the free and the bound forms are equal ($D_{B,i} = D_{CaB,i}$) (Wagner and Keizer, 1994). Under these conditions the partial derivatives of $[B_i]$ and $[CaB_i]$ are equal with opposite signs. For immobile binding partners, the diffusive terms vanish but the total concentration typically will be spatially non-uniform. Equations (10.19) illustrate that calcium dynamics is governed by a fairly complex coupled system of partial differential equations, which in general is difficult to solve analytically. This notion highlights the increased complexity of signaling when intracellular binding sites are present at a high density. It also indicates that it might not be intuitively clear how such a complex signaling system is perturbed by the addition of a calcium indicator. In general, Equations (10.19) can be solved numerically by discretizing them in both time and space (see for example DeSchutter and Smolen, 1998; Markram et al., 1998). Several modeling environments for simulating neuronal dynamics, for example NEURON (Carnevale and Hines, 2009) and GENESIS (Bower and Beeman, 1998), support the simulation of calcium dynamics within cell compartments of various geometries and within entire compartmental models of neurons. Because our knowledge of the identity, subcellular distribution and kinetic properties of endogenous Ca^{2+}-binding proteins in most cases is limited, realistic high-resolution simulations, attempting to take into account many details, are still difficult. On the other hand, for many applications such detail is not needed. Depending on the spatial scale of interest, one can focus on a few relevant aspects of calcium dynamics and thereby derive helpful analytical approximations, which will be further eluded on in Section 10.4.

After this introduction to the basic mechanisms governing intracellular calcium dynamics, the next section will treat the different types of fluorescence changes of calcium indicators, how they are utilized for calcium imaging, and how they can be related back to the underlying $[Ca^{2+}]_i$ changes.

10.3 Calcium-dependent fluorescence properties

Fluorescent calcium indicators translate Ca^{2+}-binding into a measurable change in fluorescence that can be read out in an optical setup. In principle, Ca^{2+}-binding may affect various fluorescence properties, including absorption or emission spectra, overall fluorescence yield, and fluorescence lifetime. Moreover, FRET indicators are designed to show large changes in FRET efficiency because of the Ca^{2+}-sensitive spacing between the two coupled fluorophores. Which of the induced changes are most suitable for reporting $[Ca^{2+}]_i$ changes depends on the specific indicator molecule as well as on the complexity of the imaging setup. In any case, the observed fluorescence changes need to be quantified, normalized,

and – if the absolute $[Ca^{2+}]_i$ values are relevant – calibrated in terms of absolute concentration levels.

10.3.1 Fluorescence intensity

The foremost readout mode of calcium indicators is a change in fluorescence intensity. Figure 10.4 illustrates a few typical cases schematically. Calcium indicator dyes can be excited by absorption of either a single or multiple photons. For example, two-photon excitation involves near-simultaneous absorption of two lower energy photons, a non-linear excitation mode that is highly suitable for deep imaging in biological tissues (Helmchen and Denk, 2005). Possible spectral effects of Ca^{2+}-binding include scaling of the emission spectrum and spectral shifts of either

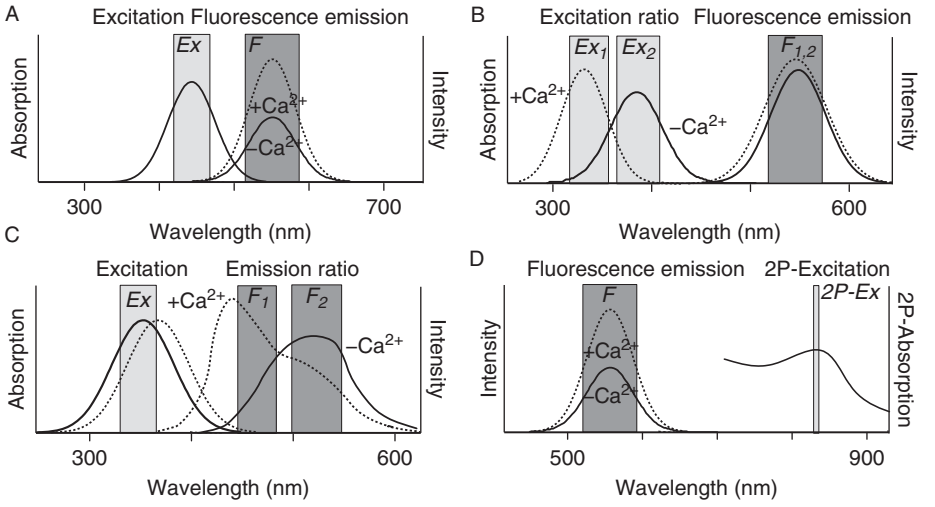

Figure 10.4 Common modes for measuring fluorescence changes of calcium indicators. A. Intensity measurement for indicators that scale their fluorescence spectrum upon Ca^{2+}-binding, showing either an increase (as illustrated here) or a decrease in fluorescence. The two boxes schematize spectral windows for excitation (*Ex*) and fluorescence collection (*F*), respectively. Windows can be set for example using band-pass optical filters. B. Fluorescence excitation ratioing can be performed with indicators that show a strong Ca^{2+}-dependent shift of their absorption spectrum. Typically, alternating excitation in two spectral windows is used in this case. C. Fluorescence emission ratioing is possible with indicators that show a strong shift of their emission spectrum. Here, emitted fluorescence is measured separately in two spectral windows. D. Two-photon excitation of calcium indicators with a pulsed near-infrared laser (bandwidth about 10 nm). In this case emitted fluorescence is of shorter wavelength than the excitation light. The examples shown here approximate the situation for Calcium Green and Oregon Green BAPTA dyes (A), fura-2 (B), indo-1 (C), and two-photon excitation of Calcium Green or Oregon Green BAPTA dyes (D).

the excitation or the emission spectrum. In Figure 10.4A a calcium indicator is single-photon excited in the visible wavelength range and fluorescence emission is collected in a separate, longer wavelength band (spectral windows are set for instance with bandpass optical filters in the excitation and detection pathways). In the case shown here, fluorescence intensity F is indicated to increase with increasing $[Ca^{2+}]_i$ but there also exist indicators that show a decrease in fluorescence instead. In general, the absorption and emission spectra of indicators at various $[Ca^{2+}]_i$ are well characterized in vitro and are available from the suppliers; one should keep in mind, however, that spectral properties depend on ionic strength, pH and viscosity and therefore may deviate from standard conditions in the cytosolic environment.

How does the fluorescence signal F relate to the $[Ca^{2+}]_i$ level? To understand this relationship we first need to clarify how fluorescence signals are generated and detected. Let us consider a cellular compartment of volume V loaded with a generic fluorescent dye X at concentration $[X]$. For simplicity we assume illumination of a flat sheet with area A and thickness l. If the excitation intensity is I_0 then the thin sheet will absorb light according to the Beer–Lambert law

$$I_{abs} = I_0 \, (1 - 10^{-\varepsilon \, l \, [X]}) \approx I_0 \ln(10) \; \varepsilon \, l \, [X] \, , \tag{10.20}$$

where ε is the molar extinction coefficient of the dye. Extinction coefficients of calcium indicators are typically in the range 20 000–100 000 $M^{-1} \, cm^{-1}$. The approximation of a linear relationship between I_{abs} and $[X]$ is only valid if $[X] < (\ln(10)\varepsilon l)^{-1}$. Equation (10.20) thus provides an upper bound to the useful dye concentration range. For measurements on small cells with 10μm diameter, dye concentration should be well below 5–20 mM. Another constraint is that Ca^{2+}-binding ratios become substantial for Ca^{2+} indicators at relatively low concentration, in particular for high affinity indicators. This extra Ca^{2+}-buffer load potentially severely alters intracellular calcium dynamics, and high affinity indicators are therefore mostly applied at micromolar concentrations.

The excited molecules within V will emit fluorescence photons isotropically with a quantum yield Q_F. The quantum yield is defined as the ratio of the number of photons emitted to the number of photons absorbed. Only a certain fraction of the emitted photons (Φ_D) is collected by the photodetection system and these photons are detected with a limited likelihood given by the detector's quantum efficiency Q_D. Taking all these factors into account, we can express the fluorescence readout signal as

$$F = Q_D \Phi_D Q_F \; I_{abs} \; = Q_D \Phi_D \, Q_F \; I_0 \, \ln(10) \, \varepsilon \, l \; [X] = S \cdot [X] \, . \tag{10.21}$$

Here, all dye- and setup-specific factors have been merged into a single proportionality constant S. For a calcium indicator we need to consider both the free and the Ca^{2+}-bound form at concentrations [B] and [CaB], respectively. They are treated as two different molecular species because they differ with respect to quantum yield and absorption properties and therefore contribute to F with different factors S_f and S_b, respectively:

$$\begin{aligned} F &= S_f\ [\mathrm{B}] + S_b\ [\mathrm{CaB}] \\ &= F_{min} + (S_b - S_f)\ [\mathrm{CaB}] \\ &= F_{max} - (S_b - S_f)\ [\mathrm{B}]\,. \end{aligned} \tag{10.22}$$

By rearranging this equation we have introduced the minimal and maximal fluorescence values $F_{min} = S_f[\mathrm{B}]_T$ and $F_{max} = S_b[\mathrm{B}]_T$ (assuming an increase in fluorescence upon Ca^{2+} binding). The ratio of these two parameters $R_f = F_{max}/F_{min}$ determines the maximal possible fluorescence change and is referred to as the *dynamic range* of the indicator. Note that the dynamic range depends on dye properties and also on the experimental setup, for example, the spectral windows used for excitation and fluorescence detection.

In the intermediate range, between F_{min} and F_{max}, the measured fluorescence intensity depends on the relative amounts of Ca^{2+}-bound and unbound indicator, which are determined by the indicator's affinity according to Equation (10.3) or (10.7). For 1:1 complexation we can convert F to $[Ca^{2+}]_i$ by expanding the fraction in Equation (10.3) and then substituting Equations (10.22):

$$[\mathrm{Ca}] = K_d \frac{[\mathrm{CaB}]\ (S_b - S_f)}{[\mathrm{B}]\ (S_b - S_f)} = K_d \frac{F - F_{min}}{F_{max} - F}. \tag{10.23}$$

This equation is the basic conversion equation for relating the measured fluorescence intensity to the intracellular calcium concentration. However, although useful for cuvette measurements (e.g. measurements of cell suspensions or calibration solutions), Equation (10.23) turns out to be impractical for imaging experiments because the optical path length, total dye concentration, and illumination intensity – and consequently F_{min} and F_{max} – usually vary over the field of view. A calibration of these parameters for each imaging pixel is not feasible. To overcome this problem various ratioing approaches are commonly employed which we describe in the next sections.

10.3.2 Relative fluorescence change $\Delta F/F$

The simplest way to account for spatial inhomogeneities is to normalize the time-dependent fluorescence change $F(t)$ to the initial baseline fluorescence

F_0 (Figure 10.5A), which yields the relative percentage change in fluorescence intensity $\Delta F/F$ (read "delta F over F"):

$$\Delta F/F = (F - F_0)/F_0. \tag{10.24}$$

Equation (10.24) as written here assumes that background fluorescence values are already subtracted from both F and F_0 beforehand. Optical components, the bathing solution and endogenous fluorophores all add background to the indicator fluorescence. Thus, the readout values from the photodetector always contain a background component that must be subtracted ($F = F_{observed} - F_{background}$). If background subtraction is omitted, $\Delta F/F$ calculated from Equation (10.24) will

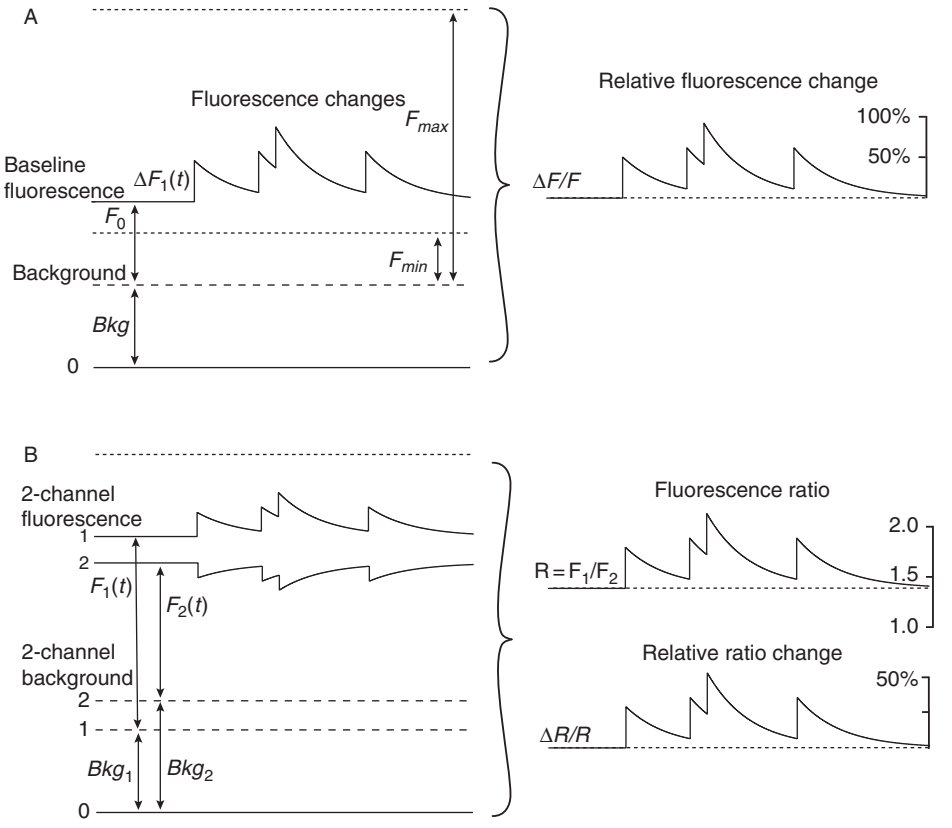

Figure 10.5 Standard methods to normalize fluorescence changes. A. The relative fluorescence change $\Delta F/F$ is calculated by dividing the background-corrected fluorescence trace by the background-corrected baseline fluorescence. $\Delta F/F$ is typically expressed as percentage change. B. For ratiometric measurements the ratio R of the background-corrected fluorescence intensities for the two channels is calculated. Note that the background needs to be determined separately for each channel. Often the change in ratio is expressed as percentage change $\Delta R/R$.

be too small, underestimating the true percentage changes. Background correction may seem trivial but actually often is not straightforward. For example, bulk-loading with AM-ester calcium indicators leads to a widespread, rather diffuse staining, for which it is difficult to obtain a good estimate of the true fluorescence background. A novel method to estimate background values, based solely on the dynamics of pixel intensities within a region of interest (ROI) can help to solve this problem (Chen et al., 2006).

How does $\Delta F/F$ relate to absolute $[Ca^{2+}]_i$ levels? Obviously, $\Delta F/F = 0$ corresponds to the resting $[Ca^{2+}]_i$ level. From Equation (10.23) one can derive the following conversion equation (Lev-Ram et al., 1992)

$$[\mathrm{Ca}] = \frac{[\mathrm{Ca}]_{rest} + K_d \frac{(\Delta F/F)}{(\Delta F/F)_{max}}}{(1 - \frac{(\Delta F/F)}{(\Delta F/F)_{max}})} \tag{10.25}$$

where $(\Delta F/F)_{max}$ denotes the maximal change upon dye saturation, which can be estimated for example using strong stimulation at the end of the experiment. The major drawback of Equation (10.25) and related single-wavelength equations (Vranesic and Knöpfel, 1991; Neher and Augustine, 1992; Wang et al., 1995) is that $[Ca^{2+}]_{rest}$ cannot be inferred from the fluorescence signal but needs to be determined in an independent manner, for example using a dual-wavelength ratiometric measurement (see below). If this is not possible, reasonable values of $[Ca^{2+}]_{rest}$ can be assumed (50–100 nM) given that the healthiness of cells can be assessed independently, for example based on morphological criteria or electrophysiological recording. Finally, for small fluorescence changes far from indicator saturation it may be sufficient to approximate changes in $[Ca^{2+}]_i$ by linearization of Equation (10.25)

$$\Delta\,[\mathrm{Ca}] = \frac{K_d}{(\Delta F/F)_{max}}(\Delta F/F) \quad (\Delta F/F \ll (\Delta F/F)_{max}). \tag{10.26}$$

Note that this equation provides an estimate of the *change* in calcium concentration but not of its absolute value. It assumes that $[Ca^{2+}]_{rest}$ has the same value as for the $(\Delta F/F)_{max}$ calibration measurements.

To circumvent the necessity for an independent measurement of $[Ca^{2+}]_{rest}$ and to obtain estimates of absolute concentrations rather than concentration changes, an alternative single-wavelength approach has been introduced that is based on a different rearrangement of Equation (10.23) (Maravall et al., 2000):

$$[\mathrm{Ca}] = K_d \frac{F/F_{max} - 1/R_f}{1 - F/F_{max}}. \tag{10.27}$$

Here, the idea is that the ratio of actual fluorescence F to saturating fluorescence F_{max} directly reflects the $[Ca^{2+}]_i$ level if the dynamic range R_f is known. While

R_f can be determined beforehand for a particular experimental setup, the maximal fluorescence F_{max} is best determined during or at the end of the experiment using strong stimulation to induce a indicator-saturating Ca^{2+} load.

10.3.3 Fluorescence ratio

Some indicators exhibit wavelength shifts in either the excitation or emission spectrum upon Ca^{2+} binding (Figure 10.4B and C). These spectral shifts can be exploited for $[Ca^{2+}]_i$ measurements because in this case the ratio $R = F_1/F_2$ of the fluorescence intensities measured in two different spectral windows (either for excitation or for emission detection) is $[Ca^{2+}]_i$ dependent. According to Equation (10.22) the intensities F_1 and F_2 are given by

$$\begin{aligned} F_1 &= S_{f1}\ [\mathrm{B}] + S_{b1}\ [\mathrm{CaB}] \\ F_2 &= S_{f2}\ [\mathrm{B}] + S_{b2}\ [\mathrm{CaB}]\,. \end{aligned} \tag{10.28}$$

Using these two equations and the law of mass action one arrives at the standard equation for ratiometric measurements (Grynkiewicz et al., 1985)

$$[\mathrm{Ca}] = K_{eff}\frac{R - R_{min}}{R_{max} - R} \tag{10.29}$$

where $R_{min} = (S_{f1}/S_{f2})$ and $R_{max} = (S_{b1}/S_{b2})$ denote the ratios at zero and saturating $[Ca^{2+}]_i$ level, respectively, and $K_{eff} = K_d\ (S_{f2}/S_{b2})$ is an effective binding constant. This ratiometric approach normalizes for inhomogeneities of dye concentration, optical path length, and illumination intensity. As in the case of $\Delta F/F$, background subtraction in each channel at the corresponding excitation or emission wavelengths is essential before taking the ratio (Figure 10.5B). Notably, the ratiometric method is not limited to indicators that show spectral shifts but can also be extended to mixtures of non-ratiometric dyes that result in Ca^{2+}-sensitive fluorescence ratios (Lipp and Niggli, 1993; Oheim et al., 1998).

10.3.4 Fluorescence lifetime

Changes in fluorescence lifetime can also be used to quantify Ca^{2+}-binding of the indicator (Lakowicz et al., 1992). Following an excitation pulse the decay in fluorescence intensity reflects the lifetime of the excited state of the dye molecules (Figure 10.6A). Microscopy techniques that inherently use a pulsed laser source for excitation such as two-photon laser scanning microscopy thus may easily be adapted for lifetime measurements (Wilms et al., 2006). In the simplest case, the fluorescence decay is described by a single exponential curve with a fluorescence lifetime constant τ_L, which is typically in the nanosecond range.

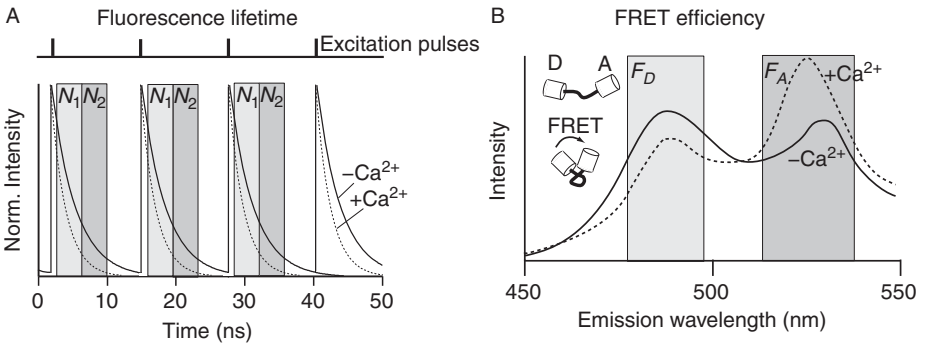

Figure 10.6 Other Ca^{2+}-dependent fluorescence properties. A. Fluorescence lifetime. Some indicators show a Ca^{2+}-dependent change in fluorescence lifetime, which is here depicted as exponential decay following each brief excitation pulse. Lifetime changes can be quantified for example by measuring the ratio of photon counts in two temporal windows (N_1, N_2) following each excitation pulse. B. FRET changes. FRET indicators utilize the Ca^{2+}-dependent change in FRET efficiency between the donor (D) and the acceptor (A) protein domain. A distance decrease between donor and acceptor leads to a decrease in detected donor fluorescence and an increase in acceptor fluorescence.

Several calcium indicators, including Fura-2, Fluo-3 and Oregon Green BAPTA-1, respond to Ca^{2+} binding with either increases or decreases in fluorescence lifetime.

Fluorescence lifetime changes can be measured using time-gated photon detection following a brief exciting laser pulse. The ratio of the numbers of photons N_1 and N_2, detected in two time windows following the excitation pulse, provides an effective fluorescence lifetime $\tau_{eff} = \Delta t / \log(N_1/N_2)$ where Δt is the width of the windows (Figure 10.6A). Both the free and the Ca^{2+}-bound form of the indicator contribute to the effective fluorescence lifetime, which relates to $[Ca^{2+}]_i$ via a equation similar to the one derived for ratiometric measurements:

$$[\mathrm{Ca}] = K_{app} \frac{\tau_{eff} - \tau_{min}}{\tau_{max} - \tau_{eff}}. \tag{10.30}$$

Here, τ_{min} and τ_{max} denote the lifetimes of the bound and free indicator forms, respectively, and K_{app} denotes an apparent dissociation constant. Alternatively, lifetime changes can be inferred from time-correlated single-photon counting with a pulsed laser source (Wilms et al., 2006) or from the phase shifts and amplitude modulation generated by a modulated light source (Lakowicz et al., 1992). Importantly, lifetimes are independent of dye concentration, optical path length, and illumination intensity and thus avoid the problem associated with a calibration based on absolute fluorescence intensities.

10.3.5 FRET efficiency

For FRET-based calcium indicators it is straightforward to adopt a ratiometric detection scheme (Figure 10.6B). Ca^{2+}-binding to the linker molecule leads to a conformational change of the entire protein such that the two interacting fluorescent proteins are brought closer together. As a result FRET efficiency increases, i.e. more energy is transferred directly from the donor protein (or protein domain) to the acceptor protein. Macroscopically this change is detectable as a reduction in donor fluorescence intensity and an increase in acceptor fluorescence. The Ca^{2+}-dependent FRET change can thus be quantified by taking the ratio R of the intensities measured in two spectral windows that reflect donor and acceptor fluorescence changes, respectively (Palmer and Tsien, 2006). Ratio changes can then be expressed as percentage changes $\Delta R/R$ relative to the baseline ratio R_0, similar to the case of $\Delta F/F$. It is also possible to use a pair of fluorescent proteins with similar emission spectra and then read out changes in FRET efficiency via fluorescence lifetime measurements (Harpur et al., 2001).

10.3.6 Calibration of calcium indicators

For some research questions it is sufficient to measure uncalibrated changes in fluorescence. For example, Ca^{2+} indicators are often employed as indirect markers of cellular or dendritic electrical excitation, which typically induces rather stereotyped Ca^{2+} influx through the activation of voltage-gated calcium channels. We will return to this type of measurement further below when we discuss how temporal patterns of action potential firing can be reconstructed from calcium imaging experiments. For this type of measurement the detection of events is the main goal and the absolute value of $[Ca^{2+}]_i$ is of secondary interest. It is nevertheless important to choose a suitable indicator with an appropriate K_d value for reporting the expected calcium transients. Even without thorough calibration, a rough estimate of the absolute changes in $[Ca^{2+}]_i$ can be obtained based on reasonable assumptions of K_d, $[Ca^{2+}]_{rest}$ and $\Delta F/F_{max}$.

Many other applications, however, do require an accurate calibration of the measured fluorescence changes in terms of absolute free Ca^{2+} concentration. For example, calibration is essential in experiments that aim to quantify the $[Ca^{2+}]_i$-dependence of specific cellular processes such as exocytosis or synaptic plasticity. The calibration procedure consists of determining the parameter sets in the above equations, (K_{eff}, R_{min}, R_{max}) or (K_d, $\Delta F/F_{max}$, $[Ca^{2+}]_{rest}$) or (K_d, R_f, F_{max}) or (K_{app}, τ_{min}, τ_{max}). For this purpose measurements with at least three calibration solutions that contain different known $[Ca^{2+}]_i$ levels are required. Note that calibration is specific to the experimental setup used and therefore cannot be transported

to other setups. Calibration measurements can be performed either "in vitro" on Ca^{2+}-buffered solutions (e.g. in small capillaries or in droplets in oil on a cover glass) or "in vivo," i.e. in living cells. A mixture of in vitro and in vivo approaches is also possible. Wherever possible, an in vivo calibration is preferable because Ca^{2+}-binding properties depend on solution properties such as its viscosity that cannot be exactly mimicked in vitro. While it is rather easy to prepare solutions that either contain no free calcium ions (through strong buffering) or saturating levels of calcium, the calibration solution with an intermediate level of $[Ca^{2+}]_i$ is most critical. The problem is that the calibration solution itself is based on a Ca^{2+} buffer (e.g. EGTA or BAPTA) and thus requires assumptions about the K_d-value of this reference buffer, which may also depend on ionic strength, pH, temperature etc. (for further reference on calibration procedures see Groden et al., 1991; Tsien and Pozzan, 1989; Neher, 2005; Palmer and Tsien, 2006; Helmchen, 2011).

Having learned about the functioning of fluorescent calcium indicators in this section, we now return to the application of simplified models of calcium dynamics to extract relevant information about neural dynamics on various spatiotemporal scales.

10.4 Simplified models of calcium dynamics

10.4.1 Calcium microdomain model

For many cellular signaling processes the exact route of calcium entry is important. The reason is that calcium-conducting channels are often strategically placed so that the activation of Ca^{2+}-binding proteins is locally restricted. Locally, $[Ca^{2+}]_i$ increases are much higher than the average ("bulk") $[Ca^{2+}]_i$ change that remains after initial concentration gradients have equilibrated by diffusion. As a consequence, the same calcium influx can exert multiple functions, activating low affinity binding proteins with subcellular specificity on the one hand and regulating distinct calcium-dependent processes with higher affinity in a more widespread fashion (Neher and Sakaba, 2008). On the molecular scale, opening of calcium-permeable ion channels causes a steep calcium concentration gradient in the immediate vicinity of the channel pores, producing "microdomains" of high $[Ca^{2+}]_i$ that develop beneath the plasma membrane (Figure 10.7A). Microdomains extend over only a few hundred nanometers with peak concentrations $>100\,\mu M$ (Neher, 1998b; Berridge, 2006) making them difficult to investigate with calcium imaging techniques (but see Llinas et al., 1992; DiGregorio et al., 1999). Calcium domains develop and collapse rapidly within a few tens or hundreds of microseconds following channel opening and closure, respectively (Roberts, 1994). At short distances the steady-state profile as a function of the radial distance r is given by

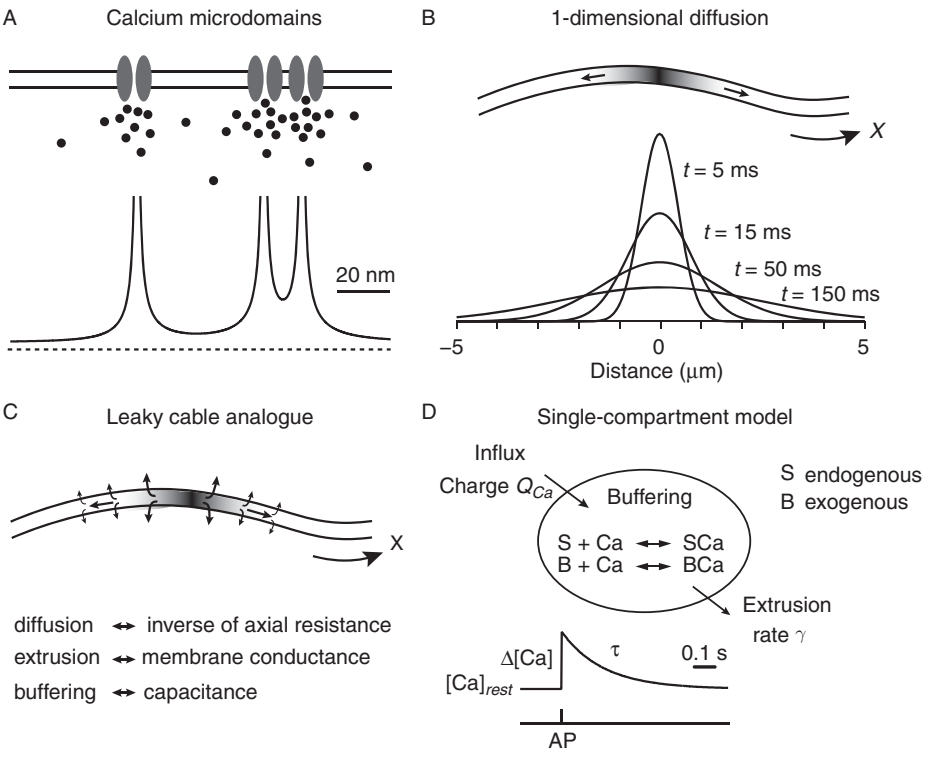

Figure 10.7 Various models of intracellular calcium dynamics. A. Calcium microdomains form beneath the mouth of open Ca^{2+}-permeable channel pores. B. Ca^{2+} redistribution in cellular processes can be modeled as one-dimensional buffered calcium diffusion. The traces show the temporal spread of Gaussian-shaped calcium concentration profiles following a localized Ca^{2+} influx. C. If Ca^{2+} extrusion mechanisms are included one obtains a leaky "chemical" cable with the main parameters bearing analogies to a passive electrical cable. D. If diffusion can be neglected the structure of interest can be considered a well-mixed compartment. In this single-compartment model, a perturbation by a brief calcium influx (e.g. during an action potential, AP) causes an exponentially shaped elementary calcium transient.

$$\Delta\,[\mathrm{Ca}]\,(r) = \frac{i_{Ca}}{4\pi F D_{Ca} r}\exp(-r/\lambda_D) \tag{10.31}$$

where i_{Ca} is the Ca^{2+} current of a single channel and λ_D is the length constant (Neher, 1986). How does the presence of Ca^{2+} buffers shape this spatial profile? While immobile Ca^{2+} buffers have no influence on the steady-state spatial profile of $[Ca^{2+}]_i$, because they bind and unbind Ca^{2+} locally at equal rates, mobile buffers have a chance to capture calcium ions near the channel, carry them away and then be replenished by free buffer molecules. Therefore they can effectively narrow the $[Ca^{2+}]_i$ profile near the channel mouth and thus restrict binding to nearby targets

(Figure 10.7A). This effect depends critically on the speed with which mobile buffer molecules capture calcium ions. Accordingly the length constant is given by (Naraghi and Neher, 1997; Neher, 1998a)

$$\lambda_D = \sqrt{D_{Ca}\ \tau_D} = \sqrt{D_{Ca}/(k_{on}\,[\mathrm{B}])} \tag{10.32}$$

where τ_D is the mean time until a calcium ion is captured by a buffer molecule and k_{on} and [B] refer to the association rate and concentration of a mobile buffer. Note that on the molecular scale binding kinetics rather than equilibrium properties of the buffer are important. As λ_D depends on the association rate, mobile buffers with either slow (e.g. EGTA) or fast (e.g. BAPTA) kinetics are differentially effective and therefore can be used to estimate the distance between intracellular targets and calcium channels (Neher, 1998a).

10.4.2 Buffered calcium diffusion

On a next higher spatial level one aims to describe Ca^{2+} redistribution in cell processes such as dendrites and axons. We consider the simple case of calcium diffusion in the presence of Ca^{2+} buffers that are either immobile or mobile. We consider only longitudinal diffusion along the axis of the process, assuming relatively thin processes. Using

$$\partial\,[\mathrm{CaB}_i]/\partial t = \kappa_{B,i}\ \partial\,[\mathrm{Ca}]/\partial t \tag{10.33}$$

we can express the sum of the partial derivatives of [Ca] and all $[\mathrm{CaB}_i]$ according to Equation (10.19) as

$$\begin{aligned}\frac{\partial\,[\mathrm{Ca}]}{\partial t} + \sum_i \frac{\partial\,[\mathrm{CaB}_i]}{\partial t} &= \left(1 + \sum_i \kappa_{B,i}\right)\frac{\partial\,[\mathrm{Ca}]}{\partial t} \\ &= D_{Ca}\frac{\partial^2\,[\mathrm{Ca}]}{\partial x^2} + \sum_i D_{B,i}\frac{\partial^2\,[\mathrm{CaB}_i]}{\partial x^2}.\end{aligned} \tag{10.34}$$

Our assumptions imply that κ_B is spatially uniform so that we can write

$$\frac{\partial^2\,[\mathrm{CaB}_i]}{\partial x^2} = \frac{\partial}{\partial x}\kappa_{B,i}\frac{\partial\,[\mathrm{Ca}]}{\partial x} = \kappa_{B,i}\frac{\partial^2\,[\mathrm{Ca}]}{\partial x^2} \tag{10.35}$$

and further simplify Equation (10.34) to

$$\left(1 + \sum_i \kappa_{B,i}\right)\frac{\partial\,[\mathrm{Ca}]}{\partial t} = (D_{Ca} + \sum_i \kappa_{B,i}\ D_{B,i})\frac{\partial^2\,[\mathrm{Ca}]}{\partial x^2}. \tag{10.36}$$

Note that on the left hand side all Ca^{2+}-binding molecules contribute, while on the right hand side only mobile buffers ($D_{B,i} \neq 0$) are relevant. The equation thus in general reduces to a simple diffusion equation

$$\frac{\partial [\mathrm{Ca}]}{\partial t} = D_{app} \frac{\partial^2 [\mathrm{Ca}]}{\partial x^2} \tag{10.37}$$

with an apparent diffusion coefficient of (Gabso et al., 1997; Irving et al., 1990; Neher, 1998a):

$$D_{app} = \frac{D_{Ca} + \sum_i \kappa_{B,i} D_{B,i}}{(1 + \sum_i \kappa_{B,i})} = \frac{D_{Ca} + \sum_j \kappa_{m,j} D_{m,j}}{(1 + \sum_j \kappa_{m,j} + \sum_k \kappa_{f,k})}. \tag{10.38}$$

Here, we highlighted the distinct roles of mobile versus immobile buffers by splitting the sums in mobile (m) and fixed (f) molecules. If only immobile Ca^{2+}-binding molecules are present, the apparent diffusion constant is reduced, i.e. calcium diffusion is effectively slowed down. Intuitively this is clear, because fixed buffers hold calcium ions in place and thus hinder their diffusional spread. If both mobile and fixed buffers are present the situation is more complex and the outcome depends critically on both the Ca^{2+}-binding ratios and the mobility of the Ca^{2+}-binding molecules. For example, if the diffusion constant of a mobile buffer is larger than the apparent diffusion coefficient in the presence of a fixed buffer ($D_{Ca}/(1 + \kappa_f)$), the addition of this mobile buffer even speeds up diffusional exchange because $D_{app} = (D_{Ca} + \kappa_m D_m)/(1 + \kappa_f + \kappa_m)$ is increased. The explanation is that a highly mobile buffer captures the substance near the source and facilitates diffusional spread by transporting it in "piggyback" fashion. In summary, intracellular buffers can both slow down and facilitate the diffusional spread of a substance depending on their concentration, affinity and mobility. This leaves room for speculation that the spatial extent of dendritic calcium compartments may not be stationary but many be dynamically regulated depending on the expression level of Ca^{2+}-binding proteins.

For the one-dimensional case considered here the well-known solution for Equation (10.37) is a spreading Gaussian shaped concentration profile (Gabso et al., 1997)

$$\mathrm{Ca}[x, t] = \frac{A_0}{\sqrt{4\pi D_{app} t}} \exp\left(-\frac{(x - x_0)^2}{4 D_{app} t}\right) \tag{10.39}$$

where A_0 indicates the strength of the pulse-like injection at time zero and position x_0 (Figure 10.7B).

10.4.3 Cable-equation analog

Most cell compartments contain effective calcium extrusion mechanisms. This is illustrated in Figure 10.7C showing a "leaky" membrane that will extrude Ca^{2+} along the cell process. If we include a simple linear removal mechanism

in Equation 10.34 – with both mobile and fixed buffers present – and rewrite the equation for concentration changes from resting level (assuming spatial homogeneity at rest), we obtain the *linearized reaction-diffusion equation*

$$\left(1+\sum_i \kappa_{m,i}+\sum_j \kappa_{f,j}\right)\frac{\partial\,\Delta\,[\mathrm{Ca}]}{\partial t} = \left(D_{Ca}+\sum_j \kappa_{m,j}D_{m,j}\right)\frac{\partial^2\Delta\,[\mathrm{Ca}]}{\partial x^2}-\gamma\,\Delta\,[\mathrm{Ca}]\,. \tag{10.40}$$

This equation is equivalent to the cable equation used to describe electrotonic spread along a cable, enabling a useful analogy between chemical and electrical signaling (Kasai and Petersen, 1994; Zador and Koch, 1994). The diffusion coefficient relates to the intracellular resistivity, the removal rate corresponds to the membrane conductance, and buffers act similar to a capacitance (for more details see Koch (1998)). In the idealized case of an infinite cylinder the chemical equivalents of space and time constants can be defined based on cable theory. The *chemical length constant* or diffusion length is given by

$$\lambda_{ch}=\sqrt{D_{app}\tau_{ch}}=\sqrt{\frac{D_{Ca}+\sum_i \kappa_{m,i}D_{m,i}}{\gamma}}. \tag{10.41}$$

with the time constant defined as

$$\tau_{ch}=\frac{1+\sum_i \kappa_{m,i}+\sum_j \kappa_{f,j}}{\gamma}. \tag{10.42}$$

Thus, the diffusion length is relatively small for a large removal rate, which could help to restrict spatially the effect of Ca^{2+} influx. Indeed, synaptic activation of aspiny dendrites of neocortical interneurons has been reported to cause localized calcium microdomains ($<1\,\mu m$) along the dendrites, which were dependent on fast Ca^{2+} influx through AMPA receptors and effective local extrusion mechanisms (Goldberg et al., 2003). On a note aside, an analogous mathematical description also holds for other intracellular signaling molecules, such as cAMP or IP_3, which however typically have longer diffusion lengths of tens of micrometers or more (Allbritton et al., 1992; Kasai and Petersen, 1994).

10.4.4 Single-compartment model

The above simplifications are useful to describe the spatiotemporal redistribution of Ca^{2+} in subcellular compartments and cell processes. Further simplification

is possible if Ca^{2+} influx occurs rather homogeneously throughout a cell compartment and diffusional equilibration is faster than Ca^{2+} extrusion. In this case diffusion can be neglected altogether (Figure 10.7D). Nearly homogeneous Ca^{2+} influx occurs, for example, when voltage-dependent Ca^{2+} channels are activated during an action potential that spreads rapidly and with little attenuation throughout the neuron. Diffusional equilibration in axonal and dendritic segments will occur within milliseconds. Even in large cell bodies initial gradients typically disappear relatively fast compared to extrusion (within less than 300 ms for a 40-μm diameter neuron; Hernandez-Cruz et al., 1990). As a first approximation we can therefore assume a stepwise homogenous increase in $[Ca^{2+}]_i$ in the initial phase. Neglecting the diffusion term in Equation (10.40) and adding repetitive Ca^{2+} influx during a train of action potentials, we obtain

$$\left(1 + \sum_i \kappa_{B,i}\right) \frac{d\,\Delta\,[\mathrm{Ca}]}{dt} = \frac{Q_{Ca}}{2FV} \sum_k \delta(t - t_k) - \gamma\,\Delta\,[\mathrm{Ca}]\,, \tag{10.43}$$

where Q_{Ca} is the Ca^{2+} charge per action potential. This balancing equation simply states that the change in total calcium concentration (left hand side, assuming constant $[Ca^{2+}]_{rest}$) equals influx minus extrusion (right hand side):

$$\frac{d[\mathrm{Ca}]_T}{dt} = \frac{d\Delta[\mathrm{Ca}]_T}{dt} = j_{in} + j_{out}. \tag{10.44}$$

Because the variable Δ[Ca] now depends only on the time variable, we have written Equation (10.44) as an *ordinary* differential equation. Assuming constant Ca^{2+}-binding ratios, the analytical solution of Equation (10.44) for a single Ca^{2+} influx is a sharp rise of $[Ca^{2+}]_i$ at time point t_0 with amplitude

$$A = \frac{Q_{Ca}/(2FV)}{(1 + \sum_i \kappa_{B,i})} \tag{10.45}$$

followed by an exponential decay with time constant

$$\tau = \frac{(1 + \sum_i \kappa_{B,i})}{\gamma}. \tag{10.46}$$

The general solution for a train of brief Ca^{2+} injections, for example as they occur during a neural spike train, is given by

$$\Delta\,[\mathrm{Ca}]\,(t) = \sum_k A\ \exp\left(-\frac{(t - t_k)}{\tau}\right)\theta(t - t_k) \tag{10.47}$$

where θ denotes the Heaviside step function. Notably, this result is equivalent to the convolution of the impulse train with an impulse response function given by a stepwise increase in amplitude A and an exponential decay with time constant τ.

For practical applications, the single-compartment model often assumes two distinct pools of rapid Ca^{2+} buffers: one pool S that represents endogenous buffers and another pool B that represents the exogenously added calcium indicator. Equations (10.45) and (10.46) can thus be rewritten as (Neher and Augustine, 1992; Regehr et al., 1994; Helmchen et al., 1996)

$$A = \frac{Q_{Ca}/(2FV)}{(1 + \kappa_S + \kappa_B)} \tag{10.48}$$

and

$$\tau = \frac{(1 + \kappa_S + \kappa_B)}{\gamma}. \tag{10.49}$$

These equations are the simplest formulation of the competition for Ca^{2+} between endogenous buffers and calcium indicator. Both A and τ depend on the Ca^{2+}-binding ratios but it is the relative amount of added buffering capacity (not its absolute value) that determines how strongly the calcium transient shape will be affected by the addition of indicator dye. Note also that the product $A\tau$ which is equal to the integral of the $[Ca^{2+}]_i$ transient (the area "underneath" the exponential curve), does not depend on Ca^{2+} binding ratios. Figure 10.8A summarizes how changes in Ca^{2+} influx, total Ca^{2+}-binding ratio and extrusion rate affect amplitude and decay time of an action potential evoked calcium transient (Sabatini and Regehr, 1995; Helmchen and Tank, 2011). While changes in influx or

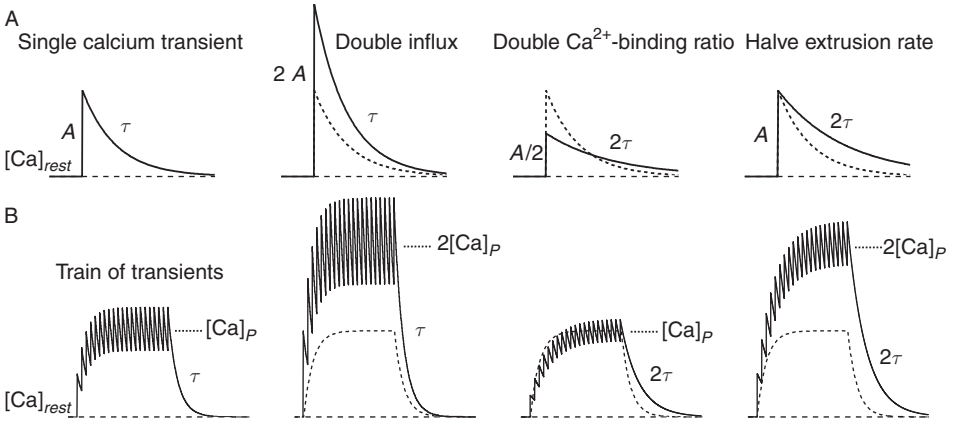

Figure 10.8 Dependence of the shape of calcium transients on the main parameters of the single-compartment model. A. Effects of doubling calcium influx, total Ca^{2+}-binding ratio, and extrusion rate on the single action potential evoked calcium transient. B. Effect of the same manipulations on the $[Ca^{2+}]_i$ accumulation during a train of action potentials at constant frequency. Note that the mean plateau level of $[Ca^{2+}]_i$ that is reached during steady state does not depend on the Ca^{2+}-binding ratio.

extrusion rate specifically alter A and τ, respectively, both parameters depend on the Ca^{2+}-binding ratio.

Because action potential evoked calcium transients are relatively slow, with typical decay times of tens to hundreds of milliseconds and even longer for cell somata, individual calcium transients summate during trains of action potentials. For rapid bursts of action potentials, Ca^{2+} influx adds up so that the calcium transient amplitude scales approximately with the number of spikes in a short burst. If spikes occur at a lower but constant frequency we can derive an analytical expression for the buildup of $[Ca^{2+}]_i$. Consider a train of stimuli starting at time $t = 0$ and with a time interval of Δt (frequency $f = 1/\Delta t$). The $[Ca^{2+}]_i$ level above resting level immediately before the $(n + 1)$th stimulus is given by a geometric progression (Regehr et al., 1994)

$$\Delta[\mathrm{Ca}](n\Delta t) = A \sum_{i=1}^{n} \exp(-(i\Delta t)/\tau) = A \frac{1 - \exp(-(n\Delta t)/\tau)}{\exp(\Delta t/\tau) - 1}. \qquad (10.50)$$

For stimulation frequencies $f < 1/(2\tau)$ there is little summation with individually spaced calcium transients, at higher frequencies calcium transients summate and $[Ca^{2+}]_i$ exponentially reaches a steady state, fluctuating around a plateau level with influx and extrusion balancing each other (Figure 10.8B). The rise time and decay of the $[Ca^{2+}]_i$ buildup in this case are governed by the time constant τ. A simple calculation reveals that the mean plateau level P that is reached at steady state is proportional to the spike frequency (Tank et al., 1995; Helmchen et al., 1996):

$$P = A\tau f \propto f \qquad (10.51)$$

with the integral $(A\tau)$ as proportionality constant. The plateau level is therefore independent of Ca^{2+}-binding ratios, which means that Ca^{2+} buffers affect the transient dynamics of $[Ca^{2+}]_i$ but not its steady-state level. The relationship between mean $[Ca^{2+}]_i$ level and the frequency of the underlying calcium influx events also indicates that intracellular calcium concentration encodes spike rate on this relatively slow time scale. Via this mechanism intracellular signaling pathways could be modulated in a spike rate dependent manner. We conclude that the single-compartment model provides a useful framework for describing the temporal pattern and the summation of elementary calcium transients.

10.4.5 Non-linear calcium dynamics

In the last sections we have introduced simplified models of intracellular calcium dynamics that are suitable to describe fluorescence measurements under various conditions. These models rely on linear approximations of the relevant processes and often assume chemical equilibrium in addition. In this section we discuss

several limitations of this approach, which are important to realize in order to understand how calcium dynamics and fluorescence measurements are affected when the assumption of linearity breaks down.

The first issue is that the approximation of constant Ca^{2+}-binding ratios is only valid for $[Ca^{2+}]_i$ changes which are small compared to the dissociation constant (Figure 10.2B). For larger changes and in particular when buffering molecules start to saturate, Ca^{2+}-binding ratios change substantially. At sufficiently high $[Ca^{2+}]_i$ levels the effective Ca^{2+}-binding ratio decreases and as a consequence $\Delta[Ca]$ induced by a certain amount of Ca^{2+} influx tends to become larger (Tank et al., 1995). Because of the overall reduced Ca^{2+}-binding ratio, decay times will also tend to become shorter. Further complexity arises from cooperative Ca^{2+}-binding due to multiple binding sites on one protein. This is relevant not only for the activation of certain intracellular enzymes, for example the Ca^{2+}-calmodulin complex (Ghosh and Greenberg, 1995), but also for the interpretation of fluorescence signals from GECIs, which typically have Hill coefficients different from unity. Indeed, non-linear response properties have been reported for various GECIs at low $[Ca^{2+}]_i$ levels, exhibiting either supralinear responses with little sensitivity for single action potentials (Pologruto et al., 2004) or single-spike sensitivity but rapid saturation with bursts of action potentials (Wallace et al., 2008).

A second important issue is saturation of Ca^{2+} extrusion mechanisms, which will lead to an opposite effect on decay time constant compared to buffer saturation, that is a prolongation rather than shortening of decay times at very high $[Ca^{2+}]_i$ levels. In addition, pump saturation is expected to alter the linear frequency dependence of the steady-state plateau level during long stimulus trains. Since buffer and pump saturation in most situations are likely to occur in parallel, the net effect may be difficult to predict. Moreover, cells typically contain a mixture of different Ca^{2+} extrusion mechanisms with distinct affinities (e.g. plasma membrane Ca^{2+}-ATPase, Na^{+}-Ca^{2+}-exchanger, and ATPases in intracellular organelles), which eventually makes detailed modeling of such a complex Ca^{2+} removal system necessary.

Another assumption in the above models (except for the calcium microdomain model) is that at any location within the cytosol, chemical equilibration is reached virtually instantaneously. However, the kinetics of Ca^{2+}-binding is not infinitely fast and thus cannot always be neglected, especially not when Ca^{2+}-binding proteins with very different on-rates are mixed together. For example, the addition of slow Ca^{2+}-binding molecules such as EGTA was found to have little effect on the amplitude of action potential evoked calcium transients but a marked acceleration of the initial decay (Atluri and Regehr, 1996; Markram et al., 1998). In contrast, addition of BAPTA at similar concentrations reduced amplitudes and prolonged

decay times as expected from the extra Ca^{2+}-binding ratio. The differential effect of EGTA and BAPTA can only be explained by their different Ca^{2+}-binding rates. Initially, calcium ions escape binding to EGTA because of its slow on-rate. Only in a second phase do calcium ions shift to EGTA molecules until these eventually have received their equilibrium share. As a result, calcium transients measured with calcium indicators, which typically belong to the pool of fast buffers, show a multi-exponential decay time course. The initial decay is governed by slow Ca^{2+} binding to EGTA acting as an additional sink, yielding an approximate fast time constant (Atluri and Regehr, 1996)

$$\tau_{fast} = \frac{(1 + \sum_i \kappa_i)}{\gamma + k^{on}_{EGTA}[\mathrm{EGTA}]}. \tag{10.52}$$

Here, the sum runs over all rapid buffers. The slow second decay phase is described by the equilibrium expression, now including the Ca^{2+}-binding ratio of EGTA:

$$\tau_{slow} = \frac{(1 + \kappa_{EGTA} + \sum_i \kappa_i)}{\gamma}. \tag{10.53}$$

This example illustrates how important kinetic effects can be, especially when multiple molecules with different binding kinetics (and possibly differential strategic localizations) are present (Markram et al., 1998). Proteins with slow binding kinetics may be bypassed altogether in the case of brief and localized Ca^{2+} influx while they can still be activated significantly during long, sustained influx. Hence, the exact spatiotemporal pattern of Ca^{2+} binding (and thus the pattern of target activation) can be a complicated function of the properties of all Ca^{2+} binding partners, which in the end needs to be explored in numerical simulations.

In summary, this section has shown that starting from a full description of intracellular calcium dynamics, certain aspects of the dynamics can be emphasized and molded in simplified models depending on the specific scientific questions of interest. Similarly, the application of calcium indicators can be tuned to uncover various aspects of neural function as will be shown in the next section.

10.5 Application modes

Calcium indicators are applied in various ways and for many purposes. In this section we discuss a few principal modes of application, which use the insights from the above theoretical considerations. One common topic is that, having realized that calcium indicators inevitably affect intracellular calcium dynamics, we can use these perturbations to our advantage for a systematic and quantitative characterization of certain aspects of calcium dynamics.

10.5.1 How to estimate unperturbed calcium dynamics

Because of the interference of calcium indicators with intracellular calcium handling it is not a trivial task to determine the unperturbed temporal dynamics of $[Ca^{2+}]_i$ as it occurs under physiological conditions. The concentration of indicator cannot be lowered infinitely in order to minimize perturbation effects because the signal to noise ratio of the fluorescence measurement will become too low. Moreover, there is no general rule on which absolute dye concentration is sufficiently low because the amount of perturbation also depends on cell properties, in particular the endogenous Ca^{2+}-binding ratio. A simple method to test whether addition of indicator severely affects the $[Ca^{2+}]_i$ measurements is to perform measurements at twice the concentration. If amplitudes and decay time constant change little, this would show that the indicator is interfering little at the original concentration. In extension of this approach, a systematic variation of the indicator concentration can be performed, from which unperturbed amplitude and decay time constants can be determined via extrapolation to zero indicator concentration (Figure 10.9). Such an approach is particularly helpful when investigating reproducible, stimulus evoked calcium influx such as during an action potential (Neher and Augustine, 1992; Helmchen et al., 1996, Helmchen et al., 1997). As an alternative, one can compare several indicators with very different Ca^{2+}-binding affinities under comparable conditions. At the same concentration, a low affinity indicator (e.g. MagFura-2) adds much less Ca^{2+}-binding ratio to the cell than its high affinity analog and therefore perturbs the cytosolic calcium dynamics much less. On the other hand, even though the fluorescence yield might be large, the evoked fluorescence changes will tend to be very small ($<1\%$) so that averaging of many trials may be necessary to resolve small calcium transients clearly (Helmchen et al., 1997).

10.5.2 How to estimate the endogenous calcium binding ratio

The systematic variation of calcium indicator concentration also enables the estimate of the endogenous Ca^{2+}-binding ratio κ_S and the clearance rate γ. For this purpose we assume the single-compartment model and plot the decay time constant of stereotype calcium transient as a function of exogenous Ca^{2+}-binding ratio κ_B (Figure 10.9A). According to Equation (10.49) this relationship is described by a linear function

$$\tau = a_1 \kappa_B + a_0 \tag{10.54}$$

with

$$\begin{aligned} a_1 &= 1/\gamma \\ a_0 &= (1 + \kappa_S)/\gamma. \end{aligned} \tag{10.55}$$

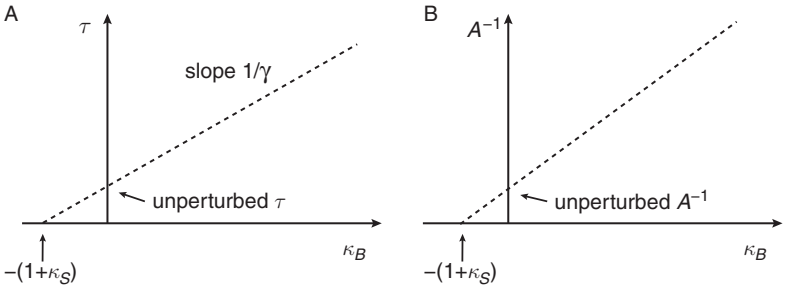

Figure 10.9 Estimate of unperturbed calcium dynamics and endogenous Ca^{2+}-binding ratio by systematically varying the indicator concentration. A. Fitting a linear relationship to a plot of decay time constant versus exogenous Ca^{2+}-binding ratio κ_B reveals the unperturbed time constant and the endogenous Ca^{2+}-binding ratio κ_S from the y- and x-axis interception, respectively. B. Similarly, a plot of the inverse of the calcium transient amplitude A versus κ_B reveals the unperturbed amplitude and κ_S from the y- and x-axis interception, respectively.

Thus, the inverse of the measured slope (a_1) provides an estimate of the clearance rate and the negative x-axis intercept ($-a_0/a_1$) provides an estimate of the endogenous buffer capacity κ_S (Neher and Augustine, 1992; Helmchen et al., 1996). Similarly, the unperturbed amplitude of the calcium transient can be estimated from a plot of the inverse of the amplitude A^{-1} versus κ_B by extrapolation (Figure 10.9B).

In practice, mainly two methods have been employed to vary the calcium indicator concentration systematically. First, whole-cell patch clamp recordings can be obtained with pipette solutions containing known indicator concentrations (alternatively, injections through intracellular sharp microelectrodes can be used but then concentrations have to be inferred indirectly from the fluorescence intensity values after loading (Tank et al., 1995)). With sufficiently low access resistance and after some waiting period one can assume diffusional equilibration between the pipette and the cell compartment. The plots in Figure 10.9 can then be built up from measurements on many cells with different indicator concentrations (Neher and Augustine, 1992; Helmchen et al., 1996; Maravall et al., 2000; Sabatini et al., 2002). A second more efficient method is to monitor the effect of adding calcium indicator during the dye loading process in individual experiments (Neher and Augustine, 1992; Helmchen et al., 1996; Sabatini et al., 2002). This approach avoids cell-to-cell variability. The actual indicator concentrations at the various measurement time points are back-calculated from the final fluorescence intensity of the cell, which is presumed to reflect complete loading with a concentration equal to the pipette concentration. With this approach κ_S can thus be estimated from single experiments. The endogenous Ca^{2+}-binding ratio κ_S has been determined for

a variety of cell types and subcellular compartments and typically yielded values between 50 and 1000 (for a summary see Helmchen and Tank, 2011).

10.5.3 How to quantify total calcium fluxes

An estimation of unperturbed calcium dynamics is important for revealing $[Ca^{2+}]_i$ changes under physiological conditions. A different goal that requires a different approach is to quantify the total Ca^{2+} flux (Schneggenburger et al., 1993; Neher, 1995). For this purpose one can load excess amounts of calcium indicator into the cellular compartment, so that the indicator molecules outcompete any other endogenous Ca^{2+} buffers and capture virtually all calcium ions. As a result the change in absolute fluorescence intensity under these "overload" conditions directly reflects the total calcium charge that has entered the cytosol. In a sense the situation is analogous to the different modes of electrical recording (Neher, 1995): while the "minimal indicator concentration" approach corresponds to "voltage recording" (or "current clamp" mode), with the aim of minimally perturbing the observable (membrane potential and $[Ca^{2+}]_i$, respectively), "indicator overload" corresponds to "voltage clamp" mode, where one variable is forced artificially to a constant value in order to gain valuable information about another variable. In the case of dye overload, $[Ca^{2+}]_i$ is effectively clamped to a low concentration while any extra Ca^{2+} influx is reported through a fluorescence change.

Mathematically we can treat the indicator overload situation as follows. From Equations (10.12) and (10.22) we see that under these conditions the evoked fluorescence change is directly proportional to the total calcium charge Q_{Ca} that has entered the cell

$$\Delta F = (S_b - S_f)\Delta\,[\mathrm{CaB}] \cong (S_b - S_f)\Delta\,[\mathrm{Ca}]_T = \frac{(S_b - S_f)}{2FV} Q_{Ca}. \qquad (10.56)$$

The proportionality constant often is defined as f_{max} (Schneggenburger et al., 1993)

$$\Delta F = f_{max}\, Q_{Ca}. \qquad (10.57)$$

If f_{max} is known one thus has a direct readout of the integral of the Ca^{2+} influx that has occurred during a certain time period. In order to use this equation the experimental setup needs to be calibrated, however, by measuring fluorescence changes that are induced by known calcium fluxes. This can be achieved, for example, by simultaneous electrical recordings of pure calcium currents (Schneggenburger et al., 1993; Helmchen et al., 1997). It should be noted, however, that ΔF is measured at one wavelength (non-ratiometric) and that S_b and S_f depend on features of the imaging setup, in particular on the illumination power, which may change over

time due to lamp aging. Therefore, regular measurements on some fluorescence standard (e.g. fluorescent beads) should be used to normalize for changes in illumination power over the course of experiments. The overload method has been applied for instance to quantify fractional Ca^{2+} currents through ligand-gated ion channels (Schneggenburger et al., 1993; Garaschuk et al., 1996; Bollmann et al., 1998) and the total calcium influx during an action potential (Helmchen et al., 1997; Bollmann et al., 1998).

10.5.4 How to characterize calcium-dependent processes

Ca^{2+}-dependent intracellular signaling pathways underlie many fundamental cell functions. To understand fully the molecular mechanisms involved we need to characterize the Ca^{2+} sensitivity of the relevant Ca^{2+}-sensing proteins in the living cell. For cellular processes, which essentially "see" the average "global" $[Ca^{2+}]_i$ changes, such as for example short-term facilitation or the recruitment of synaptic vesicle pools (Neher and Sakaba, 2008), the required measurements can be made with a well-calibrated calcium imaging setup and do not require particularly high spatial resolution. However, many other processes sense the local rather than global $[Ca^{2+}]_i$ changes and it is therefore difficult if not impossible to apply calcium imaging techniques for quantitative measurements on this scale. Calcium sensors are often anchored to protein complexes and placed strategically in the vicinity of calcium sources. For example, neurotransmitter release is triggered by localized calcium influx through voltage-gated calcium channels positioned very close to the presynaptic protein complexes triggering vesicle fusion with the membrane (Neher and Sakaba, 2008). Precise optical measurements of the absolute changes in Ca^{2+} concentration reached within calcium microdomains are beyond what optical imaging technology currently can achieve. Perhaps novel nanoresolution light microscopy techniques (Hell, 2007) in the future will enable functional calcium measurements with a spatial resolution below 100 nm, but even then the effective Ca^{2+} concentration at the proteins of interest will be hard to determine. Analysis of local $[Ca^{2+}]_i$ values is further hindered by the complicated effects that the indicator molecules have on intracellular calcium dynamics on this molecular scale.

A method to circumvent these problems is flash photolysis of caged calcium compounds (Neher and Zucker, 1993). In this approach, a brief flash of light causes release of Ca^{2+} from the caged compound by rapidly changing its affinity for Ca^{2+}-binding. The goal is to increase the average cytosolic Ca^{2+} concentration uniformly in a step-like fashion and to quantify the absolute $[Ca^{2+}]_i$ level reached using a simultaneous measurement with a fluorescent calcium indicator. At the same time the resulting action of Ca^{2+}-binding (e.g. induction of a postsynaptic

current) is read out and quantified. Because flash photolysis leads to a spatially homogenous elevation of $[Ca^{2+}]_i$ it circumvents the problem of highly localized calcium domains. More details on the principles and application of the calcium uncaging technique, in particular its use for quantifying the calcium dependence of neurotransmitter release at central synapses, can be found in recent reviews (Schneggenburger and Neher, 2005; Neher and Sakaba, 2008).

10.5.5 How to reconstruct neural spike trains

The prospect of optical measurement of the spiking activity in large neuronal networks has fascinated researchers for many years. While membrane potential imaging using voltage-sensitive dyes still suffers from low signal to noise ratios and difficulties in achieving single-trial measurements in intact tissue, calcium imaging offers a promising alternative by providing an indirect measure of action potential firing. For a given cell type, each action potential elicits a stereotype Ca^{2+} influx in the soma (and dendrites), which induces an elementary calcium transient. We neglect here subtle frequency-dependent changes in Ca^{2+} influx and we also neglect potential other sources of calcium, for example, release from intracellular stores. The total amount of Ca^{2+} influx depends on action potential shape as well as on the density of voltage-gated calcium channels and therefore may vary between different cell types. The duration of the evoked calcium transients is typically much longer than the Ca^{2+} influx itself, with the activity of extrusion mechanisms and the total Ca^{2+}-binding ratio as main determinants of the decay time course. The main issue is that for specific experimental conditions each cell type displays a characteristic "impulse response," given by the single action potential evoked calcium transient $C_1(t)$. For a train of n action potentials the time course of the resulting $[Ca^{2+}]_i$ change $C_n(t)$ is a filtered version of the action potential train A_n or – mathematically more precise – it is the convolution of the spike train A_n with the impulse response $C_1(t)$ (Figure 10.10)

$$C_n(t) = C_1(t) * A_n(t). \tag{10.58}$$

For an action potential train with spike times t_k $(k = 1, \ldots, n)$ and assuming a single-exponentially decaying elementary calcium transient, this equation is equivalent to the expression that was given in Equation (10.47). Note that in general more complex elementary calcium transients with several decay components or a slow onset (filtered for example by dye kinetics or by the time it takes Ca^{2+} to equilibrate by diffusion throughout a large cell compartment) may need to be assumed.

In practice, fluorescence measurements using fluorescent calcium indicators are always confounded by experimental noise (Figure 10.10). In more general terms we thus have to write

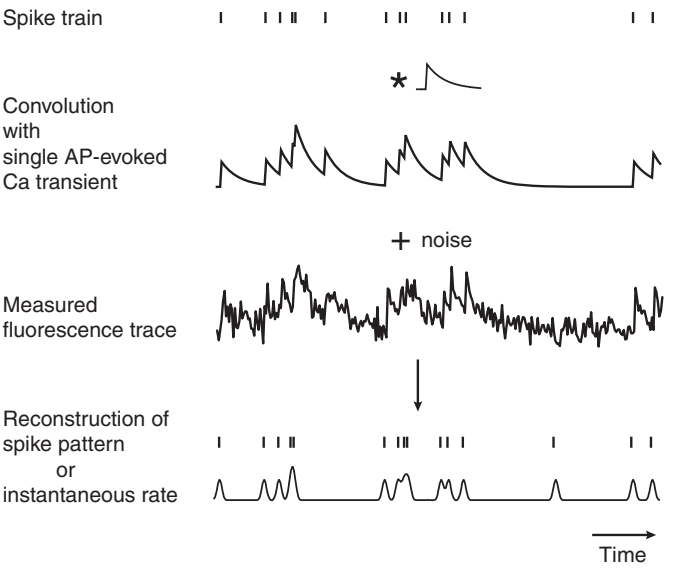

Figure 10.10 Reconstruction of neuronal spike trains from calcium indicator fluorescence measurements. Assuming a strict relationship between action potentials and evoked calcium influx, the fluorescence time course reflects the convolution of the spike train with the single action potential evoked calcium transient as "impulse response". Depending on the level of experimental noise, various methods can be used to reconstruct more-or-less accurately the spike train or the time course of instantaneous spike rate. Note a missed spike and the occurrence of a false-positive spike in the schematic example shown here.

$$C_n(t) = C_1(t) * A_n(t) + N(t). \tag{10.59}$$

The noise term $N(t)$ may originate from various sources, including detector noise and photon shot noise. In order to reveal the dynamic pattern of action potential firing in an entire neuronal population, we face the challenge of reconstructing (or "deconvolving") the action potential train in each cell and of finding the best estimate for the spike pattern underlying the observed noisy fluorescence traces. The temporal precision of such a reconstruction is clearly limited by the acquisition rate of the imaging system and in most cases is far from reaching millisecond accuracy. For many purposes it may be sufficient, however, to reconstruct the temporal dynamics as instantaneous spike rate, which is a smooth function "blurred" over a certain temporal window.

Several algorithms have been proposed for the reconstruction of action potential patterns from fluorescence traces (see for example Smetters et al., 1999; Ramdya et al., 2006; Yaksi and Friedrich, 2006; Kerr et al., 2007; Moreaux and Laurent, 2007; Holekamp et al., 2008; Greenberg et al., 2008; Sasaki et al., 2008; Vogelstein et al., 2009, 2010; Grewe et al., 2010). Here we only introduce a

basic approach using the Wiener filter as deconvolution filter (Press et al., 1988). The task is to find an optimal solution for $A_n(t)$ given the noisy $C_n(t)$. Rewriting Equation (10.59) in Fourier space transforms the convolution operation into a multiplication and yields

$$\hat{C}_n(\omega) = \hat{C}_1(\omega) \cdot \hat{A}_n(\omega) + \hat{N}(\omega). \tag{10.60}$$

In the presence of "white noise" the optimal filter for retrieving $A_n(\omega)$ in the Fourier domain is (Press et al., 1988)

$$\hat{A}_n(\omega) = \hat{H}(\omega)\, \hat{C}_n(\omega) \tag{10.61}$$

where $H(\omega)$ is the Wiener filter given by

$$\hat{H}(\omega) = \frac{\hat{C}_1(\omega)}{\left|\hat{C}_1(\omega)\right|^2 + \left|\hat{N}(\omega)\right|^2} = \frac{\hat{C}_1(\omega)}{\left|\hat{C}_1(\omega)\right|^2 (1 + \alpha(\omega))} \tag{10.62}$$

with $\alpha = |N(\omega)|^2/|C_1(\omega)|^2$. Inverse fourier transformation of $A_n(\omega)$ then yields an estimate for the original spike train $A_n(t)$. $N(\omega)$ may be estimated from the noise spectrum in the absence of neural activity and $C_1(\omega)$ from the assumed model of elementary calcium transient. Alternatively the parameter α can be fine tuned empirically. Special pre-processing steps, including non-linear filters (Yaksi and Friedrich, 2006), may further increase the accuracy of the reconstruction. The Wiener filter is clearly not the best solution to this problem and can be outperformed by more sophisticated model-based approaches (Greenberg et al., 2008; Vogelstein et al., 2009, 2010), which in principle can also deal with non-linear effects such as dye saturation. With new methods for high-speed two-photon calcium imaging (Rochefort et al., 2009; Grewe et al., 2010; Rothschild et al., 2010; Cheng et al., 2011) there are also new options for spike train reconstruction with improved temporal precision. For example, using a novel "peeling" algorithm that reconstructs complex spike trains based on iterative subtraction of a template calcium transient waveform, neural spike times could be determined with near-millisecond precision (Grewe et al., 2010). An important caveat is that a one-to-one relationship between action potential firing and somatic calcium transient does not hold for all cell types; for example somatic calcium transients have been reported in granule cells of olfactory bulb upon subthreshold activation (Egger, 2007; Lin et al., 2007). For several reasons it is thus important to verify the performance and validity of a reconstruction algorithm using simultaneous electrical and optical recordings, also allowing the quantification of success rate and rate of false positives/negatives (Kerr et al., 2005; Sasaki et al., 2008; Grewe et al., 2010). Further progress in calcium indicator performance and imaging techniques in the

near future is likely to drive optimization of the methods for optical reconstruction of neural spike trains from calcium imaging data, especially under in vivo conditions.

10.6 Comparison with other techniques

With the large toolbox of fluorescent calcium indicator now at hand and with the continual progress of in vivo labeling techniques, calcium imaging currently is the prevailing optical technique for studying the function of cell compartments, individual cells, and populations of cells. As a fluorescence technique that is easily implemented in high-resolution microscopes, calcium imaging has the key advantage of providing cellular and subcellular resolution. It thus complements other non-optical techniques, such as extracellular recordings, and optical techniques for functional imaging that lack cellular resolution, such as fMRI or intrinsic optical signal imaging.

Calcium imaging can provide quantitative data about the fundamental role of Ca^{2+} in various physiological processes and in different cell types. In neural tissue calcium imaging is a versatile tool for dissecting principles of neural excitation from the synaptic to the neural network level. As an imaging technique, calcium measurements are complementary to electrophysiological recordings in several ways. Imaging data can be obtained simultaneously from many recording sites, revealing spatiotemporal dynamics, and even very thin dendritic processes and synaptic structures can be investigated that are hardly accessible to recording pipettes. On the other hand the temporal resolution of calcium imaging typically is traded off against the spatial extent of sampling and in most applications is poor compared to electrophysiological recordings. Different from voltage-sensitive dye signals, calcium indicator signals are indirectly related to membrane potential changes. However, because action potential induced Ca^{2+} influx appears to be a quite universal neuronal feature and because VSD imaging still suffers from low signal to noise ratios, in vivo calcium imaging from neuronal populations is currently the most promising approach for investigating network dynamics in local neuronal microcircuits.

Another advantage of calcium imaging is that it can probe activity patterns not only in neurons but additionally in glial cells that also show $[Ca^{2+}]_i$ changes upon their activation. For example, astrocytes in the neocortex (Hirase et al., 2004; Nimmerjahn et al., 2004; Wang et al., 2006) as well as Bergmann glia in the cerebellum (Hoogland et al., 2009; Nimmerjahn et al., 2009) display spontaneous as well as sensory- or behavior-related calcium signals. The ability to monitor activation patterns simultaneously in the intermingled local networks of neurons and glial cells opens particularly interesting opportunities to study neuro–glial interactions.

I like to emphasize that many of the principles of indicator fluorescence measurements that were treated in this chapter are generally applicable and might be equally well used for interpreting fluorescence measurements with other small-molecule ion indicators or genetically encoded sensors (e.g. for Na^+, Cl^-, cAMP, etc.).

10.7 Future perspectives

Several aspects of calcium indicator measurements and their interpretation are likely to gain more interest in the near future. First, more information is needed about the differences in calcium dynamics in the various cell types, for example, the many subtypes of GABAergic neurons found in the cortical microcircuits. This will be important in order to achieve a comprehensive reconstruction of activity patterns in local populations taking all their diversity into account. Second, non-linear features of calcium indicators, such as saturation, will increasingly be considered to understand the relationship between electrical excitation, calcium concentration changes, and fluorescence signals more completely. This is particularly true for newest generation GECIs, for which the binding curves, conformational changes, and interactions with other proteins can be complex. Third, consideration of kinetic properties of calcium indicators will become essential not only when analyzing calcium dynamics on the very fine spatial scale, in synaptic and dendritic structures, but also when starting to model the multiple parallel effects of calcium influx on the cytosolic protein networks. Finally, the combination of electrical recordings – be it juxtacellular or multi-electrode extracellular recordings – will remain a key technique for verifying the interpretation of calcium measurements in terms of neuronal spiking.

The principles of calcium imaging are rather independent of the microscope setup but the interpretation of measured calcium dynamics clearly depends on specific parameters of the imaging procedure such as sampling frequency, spatial resolution, and sensitivity. Implementations of calcium imaging may crucially depend on the specific imaging technology, which is obvious in the case of two-photon calcium imaging because it is the only method that allows cellular imaging several hundred micrometers deep inside neural tissue (Helmchen and Denk, 2005; Kerr and Denk, 2008). Therefore, further advances in microscopy and labeling techniques may open entire new fields of application for calcium imaging. One promising direction is the development of three-dimensional laser scanning technologies, which enable comprehensive volumetric measurements from local cell populations and thus new insights into the fundamentals of neural network dynamics (Göbel and Helmchen, 2007b; Göbel et al., 2007). The same holds true for imaging at higher speed, which is essential to capture rapid signal flow through

neural networks (Grewe et al., 2010). Moreover, the ongoing improvement and further development of GECIs (Mank et al., 2008; Wallace et al., 2008, Lütcke et al., 2010) and their great potential for combination with other methods such as viral tracing techniques (Granstedt et al., 2009), can be foreseen to revolutionize the analysis of neural circuits in the neurosciences. Soon it will be possible to monitor neural network activity repeatedly over days to weeks from the same cell population, which will open tremendous opportunities to study the formation, plasticity, and reconfiguration of neural circuits.

After forty years of calcium imaging we are still experiencing only the beginning of the use of this powerful method for the study of cellular function. Most of the principles of fluorescence measurements that were covered in this chapter will remain valid so that we hope that young researchers have gained a solid foundation for exploring new research fields.

Acknowledgments

Work in the author's department was supported by research grants from the Swiss National Science Foundation (grants 3100A0-114624 and 310030-127091), the EU-FP7 program (projects 200873, 223524, 243914, 269921), and the Swiss SystemsX.ch initiative (Neurochoice project).

References

Allbritton, N. L., Meyer, T. and Stryer, L. (1992). Range of messenger action of calcium ion and inositol 1,4,5-trisphosphate. *Science*, **258**, 1812–1815.

Atluri, P. P. and Regehr, W. G. (1996). Determinants of the time course of facilitation at the granule cell to Purkinje cell synapse. *J. Neurosci.*, **16**, 5661–5671.

Baird, G. S., Zacharias, D. A. and Tsien, R. Y. (1999). Circular permutation and receptor insertion within green fluorescent proteins. *Proc. Natl. Acad. Sci. USA*, **96** etc., 11241–11246.

Berridge, M. J. (2006). Calcium microdomains: organization and function. *Cell Calcium*, **40** etc., 405–412.

Bollmann, J. H., Helmchen, F., Borst, J. G. and Sakmann, B. (1998). Postsynaptic Ca^{2+} influx mediated by three different pathways during synaptic transmission at a calyx-type synapse. *J. Neurosci.*, **18**, 10409–10419.

Borst, J. G. and Helmchen, F. (1998). Calcium influx during an action potential. *Methods Enzymol.*, **293**, 352–371.

Bower, J. M. and Beeman, D. (1998). *The Book of GENESIS: Exploring Realistic Neural Models with the GEneral NEural SImulation System* (2nd edition). New York: Springer Verlag.

Brown, J. E., Cohen, L. B., De Weer, P., Pinto, L. H., Ross, W. N. and Salzberg, B. M. (1975). Rapid changes in intracellular free calcium concentration. Detection by metallochromic indicator dyes in squid giant axon. *Biophys. J.*, **15**, 1155–1160.

Carnevale, N. T. and Hines, M. L. (2009). *The NEURON Book*. Cambridge: Cambridge University Press.

Chen, T. W., Lin, B. J., Brunner, E. and Schild, D. (2006). In situ background estimation in quantitative fluorescence imaging. *Biophys. J.*, **90**, 2534–2547.

Cheng, A., Goncalves, J. T., Golshani, P., Arisaka, K. and Portera-Cailliau, C. (2011). Simultaneous two-photon calcium imaging at different depths with spatiotemporal multiplexing. *Nature Methods*, **8**, 139–142.

DeSchutter, E. and Smolen, P. (1998). Calcium dynamics in large neuronal models. In: C. Koch and I. Segev (editors), *Methods in Neuronal Modeling*. Cambridge, MA: MIT Press, pp. 211–250.

DiGregorio, D. A., Peskoff, A. and Vergara, J. L. (1999). Measurement of action potential-induced presynaptic calcium domains at a cultured neuromuscular junction. *J. Neurosci.*, **19**, 7846–7859.

Egger, V. (2007). Imaging the activity of neuronal populations: when spikes don't flash and flashes don't spike. *J. Physiol.*, **582**(1), 7.

Gabso, M., Neher, E. and Spira, M. E. (1997). Low mobility of the Ca^{2+} buffers in axons of cultured Aplysia neurons. *Neuron*, **18**, 473–481.

Garaschuk, O., Schneggenburger, R., Schirra, C., Tempia, F. and Konnerth, A. (1996). Fractional Ca^{2+} currents through somatic and dendritic glutamate receptor channels of rat hippocampal CA1 pyramidal neurones. *J. Physiol. (London)*, **491**, 757–772.

Garaschuk, O., Milos, R. I., Grienberger, C., Marandi, N., Adelsberger, H. and Konnerth, A. (2006). Optical monitoring of brain function in vivo: from neurons to networks. *Pflügers Arch.*, **453**, 385–396.

Garaschuk, O., Griesbeck, O. and Konnerth, A. (2007). Troponin C-based biosensors: a new family of genetically encoded indicators for in vivo calcium imaging in the nervous system. *Cell Calcium*, **42** (4–5), 351–361.

Ghosh, A. and Greenberg, M. E. (1995). Calcium signaling in neurons: molecular mechanisms and cellular consequences. *Science*, **268**, 239–247.

Göbel, W. and Helmchen, F. (2007a). In vivo calcium imaging of neural network function. *Physiology (Bethesda)*, **22**, 358–365.

Göbel, W. and Helmchen, F. (2007b). New angles on neuronal dendrites in vivo. *J. Neurophysiol.*, **98**, 3770–3779.

Göbel, W., Kampa, B. M. and Helmchen, F. (2007). Imaging cellular network dynamics in three dimensions using fast 3D laser scanning. *Nature Methods*, **4**, 73–79.

Goldberg, J. H., Tamas, G., Aronov, D. and Yuste, R. (2003). Calcium microdomains in aspiny dendrites. *Neuron*, **40**, 807–821.

Granstedt, A. E., Szpara, M. L., Kuhn, B., Wang, S. S. and Enquist, L. W. (2009). Fluorescence-based monitoring of in vivo neural activity using a circuit-tracing pseudorabies virus. *PLoS One*, **4**, e6923.

Greenberg, D. S., Houweling, A. R. and Kerr, J. N. (2008). Population imaging of ongoing neuronal activity in the visual cortex of awake rats. *Nature Neurosci.*, **11** (7), 749–751.

Grewe, B. F. and Helmchen, F. (2009). Optical probing of neuronal ensemble activity. *Curr. Opinion Neurobiol.*, **19**, 520–529.

Grewe, B. F., Langer, D., Kasper, H., Kampa, B. M. and Helmchen, F. (2010). High-speed in vivo calcium imaging reveals spike trains in neuronal networks with near-millisecond precision. *Nature Methods*, **7**, 399–405.

Groden, D. L., Guan, Z. and Stokes, B. T. (1991). Determination of Fura-2 dissociation constants following adjustment of the apparent Ca-EGTA association constant for temperature and ionic strength. *Cell Calcium*, **12**, 279–287.

Grynkiewicz, G., Poenie, M. and Tsien, R. Y. (1985). A new generation of Ca^{2+} indicators with greatly improved fluorescence properties. *J. Biol. Chem.*, **260**, 3440–3450.

Harpur, A. G., Wouters, F. S. and Bastiaens, P. I. (2001). Imaging FRET between spectrally similar GFP molecules in single cells. *Nature Biotechnol.*, **19**, 167–169.

Heim, N. and Griesbeck, O. (2004). Genetically encoded indicators of cellular calcium dynamics based on troponin C and green fluorescent protein. *J. Biol. Chem.*, **279**, 14280–14286.

Hell, S. W. (2007). Far-field optical nanoscopy. *Science*, **316**, 1153–1158.

Helmchen, F. (2011). Calibration of fluorescent calcium indicators. In: *R. Yuste (editor), Imaging: A Laboratory Manual*. Cold Spring Harbor, NY: Cold Spring Harbor Laboratory Press.

Helmchen, F. and Denk, W. (2005). Deep tissue two-photon microscopy. *Nature Methods*, **2**, 932–940.

Helmchen, F. and Tank, D. W. (2011). A single-compartment model of calcium dynamics in nerve terminals and dendrites. In: F. Helmchen and A. Konnerth (editors), *Imaging in Neuroscience: A Laboratory Manual*. Cold Spring Harbor, NY: Cold Spring Harbor Laboratory Press.

Helmchen, F., Imoto, K. and Sakmann, B. (1996). Ca^{2+} buffering and action potential-evoked Ca^{2+} signaling in dendrites of pyramidal neurons. *Biophys. J.*, **70**, 1069–1081.

Helmchen, F., Borst, J. G. and Sakmann, B. (1997). Calcium dynamics associated with a single action potential in a CNS presynaptic terminal. *Biophys. J.*, **72**, 1458–1471.

Hernandez-Cruz, A., Sala, F. and Adams, P. R. (1990). Subcellular calcium transients visualized by confocal microscopy in a voltage-clamped vertebrate neuron. *Science*, **247**, 858–862.

Hirase, H., Qian, L., Bartho, P. and Buzsaki, G. (2004). Calcium dynamics of cortical astrocytic networks in vivo. *PLoS Biol.*, **2**, E96.

Holekamp, T. F., Turaga, D. and Holy, T. E. (2008). Fast three-dimensional fluorescence imaging of activity in neural populations by objective-coupled planar illumination microscopy. *Neuron*, **57**, 661–672.

Hoogland, T. M., Kuhn, B., Göbel, W., Huang, W., Nakai, J., Helmchen, F., Flint, J. and Wang, S. S. (2009). Radially expanding transglial calcium waves in the intact cerebellum. *Proc. Natl. Acad. Sci. USA*, **106**, 3496–3501.

Irving, M., Maylie, J., Sizto, N. L. and Chandler, W. K. (1990). Intracellular diffusion in the presence of mobile buffers. Application to proton movement in muscle. *Biophys. J.*, **57**, 717–721.

Kasai, H. and Petersen, O. H. (1994). Spatial dynamics of second messengers: IP_3 and cAMP as long-range and associative messengers. *Trends Neurosci.*, **17**, 95–101.

Kerr, J. N. and Denk, W. (2008). Imaging in vivo: watching the brain in action. *Nature Rev. Neurosci.*, **9**, 195–205.

Kerr, J. N. D., Greenberg, D. and Helmchen, F. (2005). Imaging input and output of neocortical networks in vivo. *Proc. Natl. Acad. Sci. USA*, **102**, 14063–14068.

Kerr, J. N., de Kock, C. P., Greenberg, D. S., Bruno, R. M., Sakmann, B. and Helmchen, F. (2007). Spatial organization of neuronal population responses in layer 2/3 of rat barrel cortex. *J. Neurosci.*, **27**, 13316–13328.

Koch, C. (1998). *Biophysics of Computation*. Oxford: Oxford University Press.

Lakowicz, J. R., Szmacinski, H., Nowaczyk, K. and Johnson, M. L. (1992). Fluorescence lifetime imaging of calcium using Quin-2. *Cell Calcium*, **13**, 131–147.

Lev-Ram, V., Miyakawa, H., Lasser-Ross, N. and Ross, W. N. (1992). Calcium transients in cerebellar Purkinje neurons evoked by intracellular stimulation. *J. Neurophysiol.*, **68**, 1167–1177.

Lin, B. J., Chen, T. W. and Schild, D. (2007). Cell type-specific relationships between spiking and $[Ca^{2+}]_i$ in neurons of the Xenopus tadpole olfactory bulb. *J. Physiol.*, **582** (1), 163–175.

Lipp, P. and Niggli, E. (1993). Ratiometric confocal Ca^{2+}-measurements with visible wavelength indicators in isolated cardiac myocytes. *Cell Calcium*, **14**, 359–372.

Llinas, R., Sugimori, M. and Silver, R. B. (1992). Microdomains of high calcium concentration in a presynaptic terminal. *Science*, **256**, 677–679.

Lütcke, H., Murayama, M., Hahn, T., Margolis, D. J., Astori, S., Meyer zum Alten Borgloh, S., Göbel, W., Yang, Y., Tang, W., Kügler, S., Sprengel, R., Nagai, T., Miyawaki, A., Larkum, M. E., Helmchen, F. and Hasan, M.T. (2010). Optical recording of neuronal activity with a genetically-encoded calcium indicator in anesthetized and freely moving mice. *Front. Neural Circ.*, **4**, 9.

Mank, M. and Griesbeck, O. (2008). Genetically encoded calcium indicators. *Chem. Rev.*, **108**, 1550–1564.

Mank, M., Santos, A. F., Direnberger, S., Mrsic-Flogel, T. D., Hofer, S. B., Stein, V., Hendel, T., Reiff, D. F., Levelt, C., Borst, A. et al. (2008). A genetically encoded calcium indicator for chronic in vivo two-photon imaging. *Nature Methods*, **5**, 805–811.

Maravall, M., Mainen, Z. F., Sabatini, B. L. and Svoboda, K. (2000). Estimating intracellular calcium concentrations and buffering without wavelength ratioing. *Biophys. J.*, **78**, 2655–2667.

Markram, H., Roth, A. and Helmchen, F. (1998). Competitive calcium binding: implications for dendritic calcium signaling. *J. Comput. Neurosci.*, **5**, 331–348.

Miyawaki, A. (2003). Fluorescence imaging of physiological activity in complex systems using GFP-based probes. *Curr. Opinion Neurobiol.*, **13**, 591–596.

Miyawaki, A., Llopis, J., Heim, R., McCaffery, J. M., Adams, J. A., Ikura, M. and Tsien, R. Y. (1997). Fluorescent indicators for Ca^{2+} based on green fluorescent proteins and calmodulin. *Nature*, **388**, 882–887.

Moreaux, L. and Laurent, G. (2007). Estimating firing rates from calcium signals in locust projection neurons in vivo. *Front. Neural Circ.*, **1**, 2.

Nagai, T., Yamada, S., Tominaga, T., Ichikawa, M. and Miyawaki, A. (2004). Expanded dynamic range of fluorescent indicators for Ca^{2+} by circularly permuted yellow fluorescent proteins. *Proc. Natl. Acad. Sci. USA*, **101**, 10554–10559.

Nakai, J., Ohkura, M. and Imoto, K. (2001). A high signal-to-noise Ca^{2+} probe composed of a single green fluorescent protein. *Nature Biotechnol.*, **19**, 137–141.

Naraghi, M. and Neher, E. (1997). Linearized buffered Ca^{2+} diffusion in microdomains and its implications for calculation of $[Ca^{2+}]$ at the mouth of a calcium channel. *J. Neurosci.*, **17**, 6961–6973.

Neher, E. (1986). Concentration profiles of intracellular calcium in the presence of a diffusible chelator. In: U. Heinemann, M. Klee, E. Neher and W. Singer (editors), Series 14, Calcium Electrogenesis and Neuronal Functioning. Berlin: Springer, pp. 80–96.

Neher, E. (1995). The use of fura-2 for estimating Ca buffers and Ca fluxes. *Neuropharmacology*, **34**, 1423–1442.

Neher, E. (1998a). Usefulness and limitations of linear approximations to the understanding of Ca^{2+} signals. *Cell Calcium*, **24**, 345–357.

Neher, E. (1998b). Vesicle pools and Ca^{2+} microdomains: new tools for understanding their roles in neurotransmitter release. *Neuron*, **20**, 389–399.

Neher, E. (2005). Some quantitative aspects of calcium fluorimetry. In: R. Yuste and A. Konnerth (editors), *Imaging in Neuroscience and Development: A Laboratory Manual*. Cold Spring Harbor: Cold Spring Harbor Laboratory Press, pp. 245–252.

Neher, E. and Augustine, G. J. (1992). Calcium gradients and buffers in bovine chromaffin cells. *J. Physiol. (London)*, **450**, 273–301.

Neher, E. and Sakaba, T. (2008). Multiple roles of calcium ions in the regulation of neurotransmitter release. *Neuron*, **59**, 861–872.

Neher, E. and Zucker, R. S. (1993). Multiple calcium-dependent processes related to secretion in bovine chromaffin cells. *Neuron*, **10**, 21–30.

Nimmerjahn, A., Kirchhoff, F., Kerr, J. N. and Helmchen, F. (2004). Sulforhodamine 101 as a specific marker of astroglia in the neocortex in vivo. *Nature Methods*, **1**, 31–37.

Nimmerjahn, A., Mukamel, E. A. and Schnitzer, M. J. (2009). Motor behavior activates Bergmann glial networks. *Neuron*, **62**, 400–412.

Oheim, M., Naraghi, M., Muller, T. H. and Neher, E. (1998). Two dye two wavelength excitation calcium imaging: results from bovine adrenal chromaffin cells. *Cell Calcium*, **24**, 71–84.

Palmer, A. E. and Tsien, R. Y. (2006). Measuring calcium signaling using genetically targetable fluorescent indicators. *Nature Protocols*, **1**, 1057–1065.

Palmer, A. E., Giacomello, M., Kortemme, T., Hires, S. A., Lev-Ram, V., Baker, D. and Tsien, R. Y. (2006). Ca^{2+} indicators based on computationally redesigned calmodulin-peptide pairs. *Chem. Biol.*, **13**, 521–530.

Pologruto, T. A., Yasuda, R. and Svoboda, K. (2004). Monitoring neural activity and [Ca^{2+}] with genetically encoded Ca^{2+} indicators. *J. Neurosci.*, **24**, 9572–9579.

Press, W. H., Flannery, B. P., Teukolsky, S. A. and Vetterling, W. T. (1988). *Numerical Recipes in C*. Cambridge: Cambridge University Press.

Ramdya, P., Reiter, B. and Engert, F. (2006). Reverse correlation of rapid calcium signals in the zebrafish optic tectum in vivo. *J. Neurosci. Methods*, **157**, 230–237.

Regehr, W. G., Delaney, K. R. and Tank, D. W. (1994). The role of presynaptic calcium in short-term enhancement at the hippocampal mossy fiber synapse. *J. Neurosci.*, **14**, 523–537.

Ridgway, E. B., and Ashley, C. C. (1967). Calcium transients in single muscle fibers. *Biochem. Biophys. Res. Commun.*, **29**, 229–234.

Roberts, W. M. (1994). Localization of calcium signals by a mobile calcium buffer in frog saccular hair cells. *J. Neurosci.*, **14**, 3246–3262.

Rochefort, N. L., Garaschuk, O., Milos, R. I., Narushima, M., Marandi, N., Pichler, B., Kovalchuk, Y. and Konnerth, A. (2009). Sparsification of neuronal activity in the visual cortex at eye-opening. *Proc. Natl. Acad. Sci. USA,* **106**, 15049–15054.

Rothschild, G., Nelken, I. and Mizrahi, A. (2010). Functional organization and population dynamics in the mouse primary auditory cortex. *Nature Neurosci.*, **13**, 353–360.

Sabatini, B. L. and Regehr, W. G. (1995). Detecting changes in calcium influx which contribute to synaptic modulation in mammalian brain slice. *Neuropharmacology*, **34**, 1453–1467.

Sabatini, B. L., Oertner, T. G. and Svoboda, K. (2002). The life-cycle of Ca^{2+} ions in dendritic spines. *Neuron*, **33**, 439–452.

Sasaki, T., Takahashi, N., Matsuki, N. and Ikegaya, Y. (2008). Fast and accurate detection of action potentials from somatic calcium fluctuations. *J. Neurophysiol.*, **100**, 1668–1676.

Schneggenburger, R. and Neher, E. (2005). Presynaptic calcium and control of vesicle fusion. *Curr. Opinion Neurobiol.*, **15**, 266–274.

Schneggenburger, R., Zhou, Z., Konnerth, A. and Neher, E. (1993). Fractional contribution of calcium to the cation current through glutamate receptor channels. *Neuron*, **11**, 133–143.

Schwaller, B. (2009). The continuing disappearance of "pure" Ca^{2+} buffers. *Cell Mol. Life Sci.*, **66**, 275–300.

Smetters, D., Majewska, A. and Yuste, R. (1999). Detecting action potentials in neuronal populations with calcium imaging. *Methods*, **18**, 215–221.

Stosiek, C., Garaschuk, O., Holthoff, K. and Konnerth, A. (2003). In vivo two-photon calcium imaging of neuronal networks. *Proc. Acad. Sci. USA*, **100**, 7319–7324.

Stryer, L. (1978). Fluorescence energy transfer as a spectroscopic ruler. *Annu. Rev. Biochem.*, **47**, 819–846.

Tank, D. W., Regehr, W. G. and Delaney, K. R. (1995). A quantitative analysis of presynaptic calcium dynamics that contribute to short-term enhancement. *J. Neurosci.*, **15**, 7940–7952.

Tian, L., Hires, S.A., Mao, T., Huber, D., Chiappe, M. E., Chalasani, S. H., Petreanu, L., Akerboom, J., McKinney, S. A., Schreiter, E. R. et al. (2009). Imaging neural activity in worms, flies and mice with improved GCaMP calcium indicators. *Nature Methods*, **6**, 875–881.

Tsien, R. Y. (1980). New calcium indicators and buffers with high selectivity against magnesium and protons: design, synthesis, and properties of prototype structures. *Biochemistry*, **19**, 2396–2404.

Tsien, R. Y. (1981). A non-disruptive technique for loading calcium buffers and indicators into cells. *Nature*, **290**, 527–528.

Tsien, R. Y. (1989). Fluorescent probes of cell signaling. *Annu. Rev. Neurosci.*, **12**, 227–253.

Tsien, R. and Pozzan, T. (1989). Measurement of cytosolic free Ca^{2+} with quin2. *Methods Enzymol.*, **172**, 230–262.

Vogelstein, J. T., Watson, B. O., Packer, A. M., Yuste, R., Jedynak, B. and Paninski, L. (2009). Spike inference from calcium imaging using sequential Monte Carlo methods. *Biophys. J.*, **97**, 636–655.

Vogelstein, J. T., Packer, A. M., Machado, T. A., Sippy, T., Babadi, B., Yuste, R. and Paninski, L. (2010). Fast nonnegative deconvolution for spike train inference from population calcium imaging. *J. Neurophysiol.*, **6**, 3691–3704.

Vranesic, I. and Knöpfel, T. (1991). Calculation of calcium dynamics from single wavelength fura-2 fluorescence recordings. *Pflugers Arch.*, **418**, 184–189.

Wagner, J., and Keizer, J. (1994). Effects of rapid buffers on Ca^{2+} diffusion and Ca^{2+} oscillations. *Biophys. J.*, **67**, 447–456.

Wallace, D. J., Zum Alten Borgloh, S. M., Astori, S., Yang, Y., Bausen, M., Kugler, S., Palmer, A. E., Tsien, R. Y., Sprengel, R., Kerr, J. N. et al. (2008). Single-spike detection in vitro and in vivo with a genetic Ca^{2+} sensor. *Nature Methods*, **5**, 797–804.

Wang, S. S., Alousi, A. A. and Thompson, S. H. (1995). The lifetime of inositol 1,4,5-trisphosphate in single cells. *J. Gen. Physiol.*, **105**, 149–171.

Wang, X., Lou, N., Xu, Q., Tian, G. F., Peng, W. G., Han, X., Kang, J., Takano, T. and Nedergaard, M. (2006). Astrocytic Ca^{2+} signaling evoked by sensory stimulation in vivo. *Nature Neurosci.*, **9**, 816–823.

Wilms, C. D., Schmidt, H. and Eilers, J. (2006). Quantitative two-photon Ca^{2+} imaging via fluorescence lifetime analysis. *Cell Calcium*, **40**, 73–79.

Woolf, T. B. and Greer, C. A. (1994). Local communication within dendritic spines: models of second messenger diffusion in granule cell spines of the mammalian olfactory bulb. *Synapse*, **17**, 247–267.

Yaksi, E. and Friedrich, R. W. (2006). Reconstruction of firing rate changes across neuronal populations by temporally deconvolved Ca^{2+} imaging. *Nature Methods*, **3**, 377–383.

Zador, A. and Koch, C. (1994). Linearized models of calcium dynamics: formal equivalence to the cable equation. *J. Neurosci.*, **14**, 4705–4715.